Moesin Regulates the Trafficking of Nascent Clathrin-coated Vesicles*[S]

Jonathan Barroso-González[‡§1], **José-David Machado**[§¶2], **Laura García-Expósito**[‡§3], and **Agustín Valenzuela-Fernández**[‡§4]

From the ‡*Laboratorio de Inmunología Celular y Viral,* ¶*Laboratorio de Neurosecreción,* §*Unidad de Farmacología, Departamento de Medicina Física y Farmacología, Facultad de Medicina, Universidad de La Laguna, Instituto de Tecnologías Biomédicas, Campus de Ofra s/n, Tenerife 38071, Spain*

Clathrin-coated vesicles are responsible for the trafficking of several internalized biological cargos. We have observed that the endogenous F-actin-linker moesin co-distributes with constitutive components of clathrin-coated structures. Total internal reflection fluorescence microscopy studies have shown that short interference RNA of moesin enhances the lateral movement of clathrin-coated structures and provokes their abnormal clustering. The aggregation of clathrin-coated structures has also been observed in cells overexpressing N-moesin, a dominant-negative construct unable to bind to F-actin. Only overexpressed moesin constructs with an intact phosphatidylinositol 4,5-bisphosphate-binding domain co-distribute with clathrin-coated structures. Hence, this N-terminal domain is mostly responsible for moesin/clathrin-coated structure association. Biochemical endosome fractioning together with total internal reflection fluorescence microscopy comparative studies, between intact cells and plasma-membrane sheets, indicate that moesin knockdown provokes the accumulation of endocytic rab5-clathrin-coated vesicles carrying the transferrin receptor. The altered trafficking of these endocytic rab5-clathrin-coated vesicles accounts for a transferrin receptor recycling defect that reduces cell-surface expression of the transferrin receptor and increases the amount of sequestered transferrin ligand. Therefore, we propose that moesin is a clathrin-coated vesicle linker that drives cargo trafficking and acts on nascent rab5-clathrin-coated vesicles by simultaneously binding to clathrin-coated vesicle-associated phosphatidylinositol 4,5-bisphosphate and actin cytoskeleton. Hence, functional alterations of moesin may be involved in pathological disorders associated with clathrin-mediated internalization or receptor recycling.

Clathrin-mediated endocytosis is a key process that governs the internalization of a plethora of cell-surface receptors in metazoans, such as G-protein-coupled receptors and epithelial growth factor receptors, and is essential for controlling cell integrity, division, and signaling (1–6). The dynamic process that enables clathrin-coated pits (CCPs)[5] to turn into clathrin-coated vesicles (CCVs) requires spatial coordination of several protein and lipid components working together to drive the formation and invagination of CCPs, and the subsequent scission and uncoating of CCVs (7, 8). Similarly, several lines of evidence have suggested a close association between the endocytic machinery in mammalian cells and the actin cytoskeleton (9–14).

Cortical actin dynamics is affected by cytoskeleton-associated proteins, such as those responsible for the growth and capping of actin filaments (15). Therefore, the ezrin-radixin-moesin (ERM) proteins from the band 4.1 superfamily are fundamental in determining signaling-induced cell shape, membrane-protein localization, cell adhesion, motility, cytokinesis, phagocytosis, and the integration of membrane transport with signaling pathways (15, 16). These ERM functions rely directly on their regulated and reversible link between membrane-associated proteins and the actin cytoskeleton (15). Remarkably, the F-actin-linker ezrin has recently been related to clathrin-mediated endocytosis of the α1β-adrenergic receptor, thereby contributing to receptor recycling to the plasma membrane (17). Moreover, the trafficking of some G-protein-coupled receptors seems to be regulated by the ERM linker EBP50, also known as NHERF1 (17–19). These data suggest that the interaction of EBP50 and ERM proteins is necessary for receptor recycling, although the mechanism that relates EBP50/ERM/F-actin linking and the receptor membrane traffic pathway is still unknown. It is interesting that ezrin and moesin proteins have been found to be associated with endosomes in an annexin-II-dependent manner (20). However, there were no reports indicating functional evidence for moesin involvement during CCV formation, internalization, or recycling.

[5] The abbreviations used are: CCP, clathrin-coated pit; CCV, clathrin-coated vesicle; ERM, ezrin-radixin-moesin; LCa-DsRed, clathrin light-chain a DsRed fusion protein; TIRFM, total internal reflection fluorescence microscopy; PIP₂, phosphatidylinositol 4,5-bisphosphate; siRNA, short interference RNA; Tf, transferrin ligand; TfR, Tf receptor; mAb, monoclonal antibody; polyAb, polyclonal antibody; GFP, green fluorescent protein; PBS, phosphate-buffered saline; CHC, clathrin heavy chain; EGFP, enhanced GFP; TfR-phl, TfR-phluorin; ECFP-PH, ECFP-tagged pleckstrin homology domain.

Moesin Drives Endocytic-CCV Trafficking

In the present work, we have studied the functional involvement of the F-actin-linker moesin in the trafficking of CCVs. Total internal reflection fluorescence microscopy (TIRFM) using the clathrin light-chain a DsRed fusion protein (LCa-DsRed) (21), as well as biochemical approaches, indicates that moesin is a component of the complex molecular machinery involved in the control of the trafficking of nascent moesin-associated CCVs.

EXPERIMENTAL PROCEDURES

Antibodies and Reagents—The monoclonal antibody (mAb) moesin (38/87)-sc-58806 recognizes moesin, the goat polyclonal antibody (polyAb) ezrin (C-19)-sc-6407 that recognizes ezrin and moesin, rabbit polyAb α-adaptin (M-300)-sc-10761, goat polyAb anti-rab5 (FL-205)-sc-28570, rabbit polyAb anti-rab7 (H-50)-sc-10767, mAb CD71 (3B82A1)-sc-32272 against transferrin receptor (TfR), and anti-phosphatidylinositol 4,5-bisphosphate (PIP$_2$) mAb (sc-53412), and anti-GFP rabbit polyAb (sc-8334) came from Santa Cruz Biotechnology Inc. (Santa Cruz, CA). Anti-clathrin heavy chain (CHC), anti-γ-adaptin and anti-α-tubulin mAbs, and PIP$_2$ were from Sigma-Aldrich. Secondary horseradish peroxidise-conjugated anti-mAb was from Immunotools (Friesoythe, Germany), and secondary horseradish peroxidise-conjugated anti-goat Ab was from Dako (Glostrup, Denmark). Alexa 488-conjugated transferrin (Tf), Alexa 568-labeled phalloïdin, and secondary antibodies Alexa 488- and/or Alexa 568-conjugated were from Invitrogen.

DNA Constructs—Human FL, N- and C-moesin-GFP constructs were kindly provided by Dr. Francisco Sánchez-Madrid (Universidad Autónoma de Madrid, Spain) and Dr. Furthmayr (Stanford University, CA) (22). LCa-DsRed, TfR-EGFP, and TfR-phluorin (TfR-phl) were provided by Dr. Wolfhard Almers (21) (Vollum Institute, Oregon Health & Science University, OR). ECFP-rab5, EGFP-rab7, and EYFP-rab11 were provided by Dr. Marino Zerial (Max Planck Institute of Molecular Cell Biology and Genetics, Dresden, Germany). GFP-α-adaptin construct was provided by Dr. Alexandre Benmerah (Institute Cochin, Paris, France). N-terminal ECFP-tagged pleckstrin homology domain of the phosphatidylinositol-specific phospholipase Cδ_1 (ECFP-PH) was provided by Dr. Senena Corbalán-García (Universidad de Murcia, Spain), and was used as a PIP$_2$ biosensor in the plasma membrane (23–25). All constructs were verified by digestion with restriction enzymes and automated dideoxynucleotide sequencing. The 4K/4N-moesin-GFP construct was prepared by using the QuikChange site-directed mutagenesis kit from Stratagene (Cedar Creek, TX). The oligonucleotides (sense, (5′-3′)) used for introducing the K253N/K254N and the K262N/K263N mutations in the FL-moesin-GFP-(1–578) molecule were (the changed bases are underlined) GGAACATCTCTTTCAATGATAA<u>C</u>AA<u>C</u>TTT-GTGATCAAGCCC and GTCATCAAGCCCATCGATAA-<u>C</u>AA<u>C</u>GCCCGGACTTCGTC, respectively. Both oligonucleotides were used as follows: 18 cycles, 95 °C, 50 s; 60 °C, 50 s; and 68 °C, 10 min.

Cells and Transfection—The human HeLa cell line was grown at 37 °C in a humidified atmosphere with 5% CO$_2$ in Dulbecco's modified Eagle's medium (Lonza, Verviers, Bel-

gium) supplemented with 10% fetal calf serum (Lonza), 1% of L-glutamine and 1% of the penicillin-streptomycin antibiotics. Cells were harvested and resuspended at a density of 50–70% in fresh supplemented Dulbecco's modified Eagle's medium, 24 h before cell transfection with siRNA and/or DNA construct. Specific Amaxa-kits (Amaxa GmbH, Koeln, Germany) were used for delivery of DNA constructs and/or siRNA into HeLa cells. Cells were nucleofected with 1 μM siRNA and/or 2 μg of each used DNA construct and assayed 24 h or 48 h later. None of the nucleofected protein constructs or siRNA oligonucleotides were toxic to the cells.

Immunofluorescence—Immunofluorescent HeLa cells were grown on glass coverslips. The cells were washed three times with phosphate-buffered saline (PBS) and fixed for 3 min in 2% formaldehyde in PBS. Cells were washed three times with PBS after fixation and then permeabilized with 0.5% Triton X-100 in PBS. The cells were washed with PBS after permeabilization and immunostained for 1 h at room temperature for primary antibodies diluted in PBS. The fluorophore-conjugated secondary antibody was also diluted in PBS for 1 h at room temperature. Finally, several washings with PBS were performed at room temperature. Coverslips were mounted in Mowiol-anti-fade (Dako, Glostrup, Denmark) and imaged in *xy* mid-sections in a FluoView^{TM} FV1000 confocal microscope (Olympus, Center Valley, PA), for high-resolution imaging of fixed cells. The final images were analyzed with Metamorph software (Universal Imaging Corp., Downington, PA).

Western Blotting—The extent of protein expression or gene silencing was assessed by Western blot of cell lysates. Cells nucleofected with scrambled oligonucleotides or short interference RNA (siRNA) oligonucleotides against moesin (siRNA-moesin or -moesin2) or with the different DNA constructs were lysed 24 h later at +4 °C in 1% SDS sample buffer with a protease inhibitor mixture (Roche Diagnostics GmbH, Mannheim, Germany) and homogenized by sonication. Equivalent amounts of proteins, measured using the bicinchoninic acid method (BCA protein assay kit from Pierce), were separated by SDS-PAGE, using 12% gradient gels and electroblotted onto nitrocellulose membrane (Sigma-Aldrich). Cell lysates were immunoblotted with specific antibodies, and protein bands were detected by luminescence using an ECL System (Pierce).

Messenger RNA Silencing—Alexa 546-conjugated or non-fluorescence siRNA oligonucleotides, scrambled or siRNA-moesin, were from Qiagen. siRNA-moesin was generated against the following mRNA sequence of moesin: 5′-agaucgaggaaca-gacuaa-3′. siRNA-moesin2 was generated against the following mRNA sequence of moesin: 5′-acuaacucccaagauaggcuuc-3′. Irrelevant scrambled siRNA served as a control. The siRNAs for moesin sustained specific interference of moesin protein expression for at least 72 h.

Tf Uptake and Recycling Assays—Tf internalization assay: HeLa cells nucleofected with scrambled or siRNA-moesin oligonucleotides (1.5 μM) were detached with PBS/5 mM EDTA, washed three times with PBS, and balanced for 1 h at 37 °C in Tf uptake buffer (Krebs-Hepes buffer with 2 mM of Ca^{2+}), before starting the experiment. Then, equivalent amounts of cells (1 × 10^6 cells·ml^{-1}) were kept on ice-cold Tf uptake buffer, and

incubated with 200 nM of Alexa 488-labeled Tf ligand at +4 °C for 30 min. Cells were washed in cold Tf uptake buffer to remove unbound ligand, and surface-bound fluorescent Tf was measured at +4 °C, under any experimental condition. This prebound Alexa 488-labeled Tf ligand was internalized at 37 °C for the indicated early times. Returning the samples to ice stopped the internalization of fluorescent Tf. Cells were washed with ice-cold PBS, and the remaining surface-bound Tf was removed by acid washing (PBS-glycine 150 mM, pH 2.3) for 3 min. Alexa 488-associated fluorescence Tf uptake was measured in cells by flow cytometry, and normalized by the total amount of Tf ligand prebound at +4 °C, as described (26).

Tf Recycling Assay—HeLa cells nucleofected with scrambled or siRNA-moesin oligonucleotides (1.5 μM) were detached as described for Tf uptake. Cells (1×10^6 cells·ml^{-1}) were then incubated with Alexa 488-labeled Tf (200 nM in Tf uptake buffer) at 37 °C for 30 min. Cells were put in ice-cold buffer to stop the uptake and recycling processes and washed in acidic buffer (PBS-glycine 150 mM, pH 2.3) to remove recycled surface-Tf ligand. Cells were then reincubated to 37 °C to allow the recycling of the internalized fluorescent Tf for the indicated time points. At these time points, cells were put on ice, washed with acidic buffer to remove recycled Tf from the cell surface, and fixed (in PBS/2% paraformaldehyde). The amount of the fluorescent Tf ligand remained (non-released) in cells was measured by flow cytometry and expressed as the percentage of the initial intracellular Tf amount detected in cells (100%, time 0 of recycling), in each experimental condition.

Cell Surface Expression of the TfR—To detect cell-surface TfR, cells were labeled for 1 h at +4 °C with mouse monoclonal anti-CD71 primary antibody diluted in PBS buffer, washed, and incubated 1 h at +4 °C with goat anti-mouse Alexa 568-conjugated secondary antibody. The cells were washed, fixed for 3 min in 2% paraformaldehyde, and fluorescence intensity was analyzed using FACScan (BD Biosciences, San José, CA). Data were analyzed using WinMDI 2.9 application software (1993–2000 Joseph Trotter).

TIRFM—Cells were imaged with an inverted microscope Zeiss 200 M (Zeiss, Germany) through a 1.45-numerical aperture objective (alpha Fluar, 100×/1.45, Zeiss) in a Krebs-Hepes buffer containing 2 mM Ca^{2+}. The objective was coupled to the coverslip using an immersion fluid ($n_{488} = 1.518$, Zeiss). The expanded beam of an argon ion laser (Lasos, Lasertechnik GmbH, Germany) was band-pass filtered and used to selectively excite different fluorescent proteins, for evanescent field illumination. Different filters were used for each analyzed fluorophor. The beam was focused at an off-axis position in the back focal plane of the objective. Light, after entering the coverslip, underwent total internal reflection as it struck the interface between the glass and the solution or cell at a glancing angle.

Total internal reflection generates an evanescent field that declines exponentially with increasing distance from the interface, depending on the angle at which light strikes the interface. The angle was measured using a hemicylinder, as described previously (21). The images were projected onto a back-illuminated charge-coupled device camera (AxioCam MRm, Zeiss) through a dichoric and specific band-pass filter for each fluoro-

phor. Each cell was imaged using Axiovision (Zeiss) for up to 2 min with 0.25-s exposures at 1 Hz when illuminated under the evanescent field.

Tracking Analysis of CCSs Movement by TIRFM Imaging—Tracking analysis of single LCa-DsRed-labeled structures was performed by using Metamorph. CCSs were excluded if they were larger than 0.5 μm or if they became oblong at any time. We marked the position of each tagged pit and tracked their x-y position as a function of time. The average radius for the x-y lateral trajectories of tracked CCSs were determined in single cells, as described (27), and calculated from the total number of cells analyzed by Metamorph.

TIRFM or Confocal Co-distribution Analysis—The overlap between different fluorescence molecules was determined by taking evanescent field and confocal images. The images were low-pass filtered using Metamorph. We plotted a small circle of 0.9-μm diameter around each analyzed spot and five circles outside these spots. These circles were used to calculate the local background. We drew 0.9-μm diameter circles around clathrin spots, duplicated the circles into the image of the pair molecule at identical pixel locations, and then determined whether the new circle contained a fluorescent point concentric to within 0.15 μm to quantify the degree of co-distribution of endogenous moesin with endogenous clathrin or α-adaptin molecules (by confocal), or the overexpressed fluorescent rab5, rab7, rab11, TfR, or α-adaptin molecules with LCa-DsRed-labeled CCSs (by TIRFM). Circles were scored as positive if they contained a fluorescent spot and negative if they did not. Moreover, co-localization was scored positive when the fluorescence intensity average was at least three times the standard deviation of the background. The percentage of co-distribution was determined in single cells after random co-distribution subtraction, and the average values were calculated from the total number of cells analyzed. Images were rotated 90 degrees and molecule co-distribution was calculated again, as described above, to determine that the observed correlation was not due to random signal overlap. If the observed co-localization was random, rotation of the image would not change the degree of signal overlap obtained before the rotation of the image.

TIRFM-based Analysis of the Tf Binding to Cell-surface TfR—To study the binding of the Tf ligand to TfR at the cell surface by TIRFM, Alexa 568-labeled Tf (50 nM in Tf uptake buffer (Krebs-Hepes with 2 mM of Ca^{2+})) was added at +4 °C for 30 min to control (scrambled) or moesin-silenced cells. Both of these cells transiently expressed the TfR-phl receptor. Cells were kept in starvation medium before Tf incubation, incubated on ice in Tf uptake buffer for 30 min, and washed with cold-Tf uptake buffer. After binding of Alexa 568-labeled Tf to TfR-phl, the cell-surface-associated fluorescence was analyzed by TIRFM, as described above for TIRFM co-distribution analysis.

Imaging TfR Exocytosis by TIRFM—Exocytosis of the TfR-phl receptor was monitored by TIRFM in control (scrambled) and moesin-silenced cells, both transiently overexpressing the fluorescent TfR-phl molecule. The frequency of TfR-phl exocytosis was calculated as the number of events recorded per cell for 60 s (3 frames/s), and comparing the frequency average between control and moesin-silenced cells (total events analyzed from 12 cells per each experimental condition).

Preparation of Plasma-membrane Sheets—Freshly nucleo-fected cells were grown on glass coverslips (ø, 12 mm) overnight. The coverslip was then rinsed in HEPES buffer (25 mM, pH 7.4), and put in contact with poly-L-Lysine (0.2 mg·ml-1)-precoated glass coverslip (ø, 18 mm) for 30 min at room temperature. Afterward, this coverslip sandwich was placed onto moist filter paper for 10 min without applying pressure. The sandwich was transferred to a Petri dish and filled with HEPES buffer, and the large coverslip (ø, 18 mm) was positioned on top. The coverslips were spontaneously separated while floating, thereby ripping off the cells to obtain plasma-membrane sheets on the poly-L-lysine-coated glass coverslip (ø, 18 mm), as described (28). These preparations were analyzed by TIRFM to visualize the different fluorescent nucleofected proteins at the cell surface.

PIP$_2$ Binding Assay and Dot-blot Analysis—Binding assay of FL-moesin-GFP or 4K/4N-moesin-GFP to soluble PIP$_2$ was performed with purified moesin molecules from lysates of respective nucleofected cells. Cells were lysed at +4 °C (PBS-1% Triton X-100, completed with a protease inhibitor mixture), and sonicated for 10 s. These lysates were precleared, and then incubated (500 μg of total protein) overnight at +4 °C with anti-GFP polyAb (40 μg), non-covalently complexed to protein G-Sepharose beads (100 μl). Co-immunoprecipitated proteins were washed with PBS buffer and incubated with 100 μl of soluble PIP$_2$ (0.5 mg·ml^{-1} in chloroform:methanol:1 N HCl: H$_2$O; at a volume ratio of 20:10:1:1) for 2 h at room temperature. The samples were washed with PBS and boiled in β-mercaptoethanol-Laemmli sample buffer for 1 min at 90 °C. Protein G-Sepharose beads were removed by centrifugation, and the supernatants were spotted in polyvinylidene fluoride membranes using a dot-blot apparatus (Slotblot, GE Healthcare). PIP$_2$ bands were probed with a specific anti-PIP$_2$ mAb (1:200). The dot blots were then reprobed, after membrane stripping with anti-GFP polyAb (1:200). PIP$_2$ and GFP fusion protein bands were detected by luminescence using the ECL system (Pierce).

Subcellular Fractionation and Protein Precipitation—Scrambled (control) or siRNA-moesin-treated HeLa cells (1 $\times$ 10^7 cells) were washed twice with PBS at +4 °C. Cells were gently scraped from culture plates and collected by centrifugation. They were then homogenized in 200 μl of buffer (78 mM KCl, 4 mM MgCl$_2$, 8.37 mM CaCl$_2$, 10 mM EGTA, 50 mM HEPES/KOH, pH 7.0) containing 250 mM sucrose and centrifuged at 1000 $\times$ g for 5 min. The supernatants (from scrambled or siRNA-moesin cells) were placed on a 5–20% linear Optiprep^{TM} (Nycomed, Amersham Biosciences) gradient, formed in 12 ml of the above buffer, and centrifuged at +4 °C, for 20 h at 100,000 $\times$ g, in an SW28 rotor (Beckman, Germany). Following the centrifugation, the total volume gradient was separated into 1-ml fractions, collected from top to bottom (from 5% to 20% Optiprep^{TM} concentration, respectively). The protein precipitation was as follows: the volume of each collected fraction (1 ml) was duplicated with cool acetone (1 ml, -20 °C) in acetone-compatible tubes. The samples were then vortexed and incubated for 1 h at -20 °C, and further centrifuged for 10 min at 13,000 $\times$ g. Samples were decanted, and the protein pellets were resuspended in Laemmli buffer to

be resolved by SDS-PAGE (12%) and Western blot techniques using specific antibodies.

*Statistics*—Data were compared using Student's *t* test. Asterisks indicate $p < 0.05$.

RESULTS

Moesin Co-distributes with Constitutive Components of CCSs—To study the involvement of moesin in CCV trafficking, we first analyzed the distribution of endogenous moesin with constitutive components of CCSs by using fluorescence confocal microscopy. We observed that endogenous moesin presented a punctated pattern of distribution in HeLa cells (Fig. 1), partially co-distributing with the endogenous CHC (Fig. 1*A*; quantified in Fig. 1*D*), a main component of the clathrin triskelion that forms CCPs and CCVs (29–31). We also observed a partial co-distribution of moesin with endogenous α-adaptin (Fig. 1*B*; quantified in Fig. 1*D*), a key component of the AP2 complex for CCV formation and clathrin-mediated endocytosis (32, 33). However, endogenous moesin slightly co-distributed with the γ-adaptin protein (Fig. 1*C*; quantified in Fig. 1*D*), a component of the heterotetrameric adaptor protein complex AP-1, which has been involved in mediating cargo sorting from the *trans*-Golgi network to the endosome compartment (reviewed in Refs. 34–38), as well as in promoting retrograde endosome to *trans*-Golgi network transport (39). The quantification of moesin co-distribution with these molecules was performed as indicated under "Experimental Procedures." These data indicate that a pool of endogenous moesin mostly co-distributes with specific components of CCSs that are associated with plasma membrane-derived CCSs.

Moesin Silencing Alters Movement and Causes Clustering of CCSs—To investigate the functional involvement of moesin in CCV trafficking, we first performed TIRFM experiments tracking LCa-DsRed-labeled structures in cells where endogenous moesin was silenced by siRNA (Fig. 2, *A* and *B*). We observed that overexpressed LCa-DsRed displayed a diffraction-limited punctated pattern in transfected cells (Fig. 2*C*, *white arrows* in scrambled and siRNA-moesin images), which is characteristic of CCSs (8, 21, 27, 40), as was observed with the endogenous CHC-monitored structures (Fig. 1*A*).

Moesin silencing provoked an alteration of the lateral movement of single LCa-DsRed-labeled CCSs (Fig. 2, *D–F*), without affecting the number and size of CCSs (Fig. 2*C*, see *white arrows*, and average line scans, for 200 CCSs sized < 0.5 μm, in scrambled or siRNA-moesin condition). Hence, the trajectories obtained for the lateral movement of LCa-DsRed-labeled CCSs, calculated as previously described (27), were larger in cells lacking moesin than those observed in control cells (Fig. 2, *D–F*, and supplemental Movies S1 and S2, from Fig. 2*F*). In control conditions, >60% of analyzed LCa-DsRed-labeled CCSs moved in trajectories from 0.5 μm to <1 μm (Fig. 2*D*, *scrambled bars*, and supplemental Movie S1, from Fig. 2*F*, *scrambled images*), whereas ~40% of analyzed structures moved in trajectories between 1 and 3.5 μm (Fig. 2*D*, *scrambled bars*).

As regards the cells without endogenous moesin, ~30% of analyzed CCSs moved in trajectories from 0.5 μm to <1 μm, whereas CCSs moving in trajectories from 1 μm to 6 μm accounted for ~70% of total analyzed CCSs (Fig. 2*D*, *siRNA-*
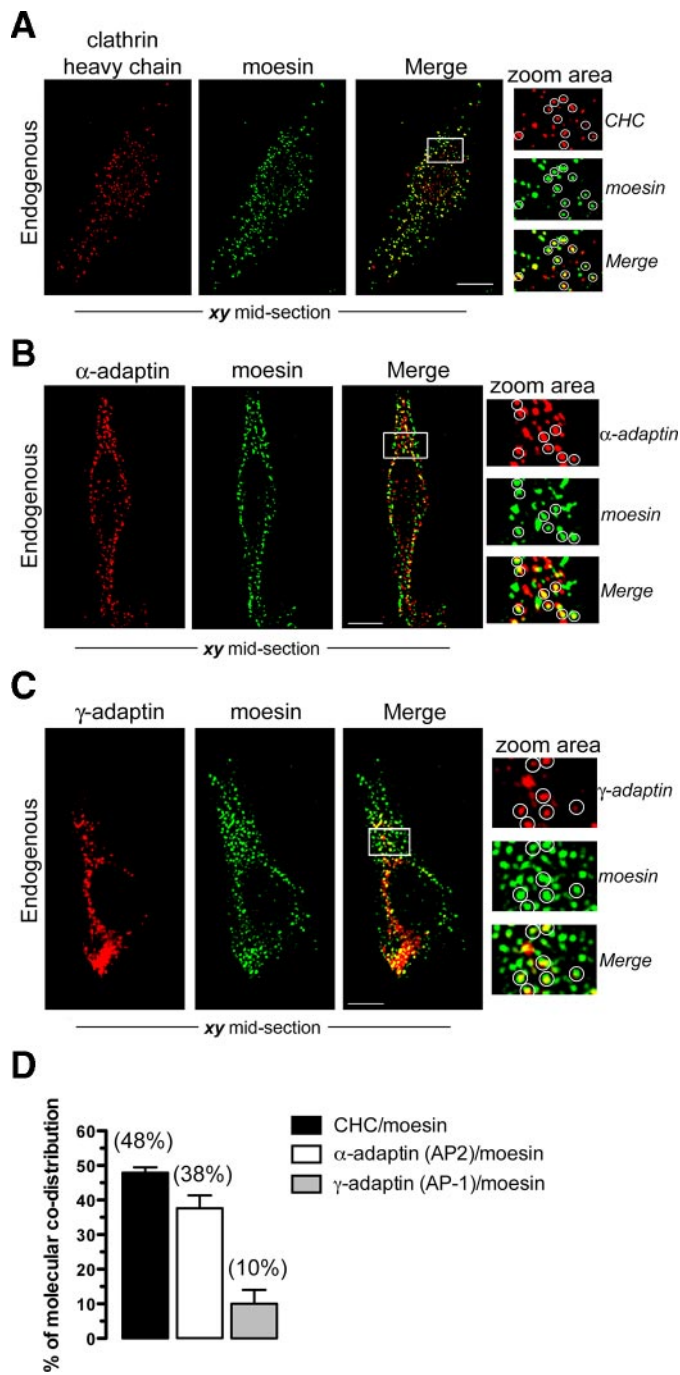
FIGURE 1. **Endogenous moesin co-distributes with components of CCSs.** *A*, confocal microscopy analysis of cellular co-distribution of endogenous CHC and moesin molecules. *B*, confocal microscopy analysis of cellular co-distribution of endogenous α-adaptin and moesin molecules. *C*, confocal microscopy analysis of cellular co-distribution of endogenous γ-adaptin and moesin molecules. From *A* to *C*, the *zoom area* shows CHC-, α-adaptin-, and γ-adaptin-labeled structures where molecule co-distribution was analyzed (*encircled vesicles* in *A*, *B*, and *C*, respectively). *D*, *bar histograms* show the quantification of the co-distribution of endogenous moesin with CHC, α-adaptin, or γ-adaptin. Data are mean ± S.E., ($n = 500$ spots from 5 different cells). The quantification was performed as described under "Experimental Procedures." *Bar*, 10 μm.

moesin bars, and supplemental Movie S2, from Fig. 2*F*, *siRNA-moesin images*). Similar results were obtained in moesin-silenced cells by using the siRNA-moesin2 oligo (supplemental Fig. S1, *A*, *Western blot* and *B*, *images*). Hence, the large trajec-

tories observed for the movement of single CCSs were from 0.5 μm to <1 μm in scrambled cells (53% of CCSs analyzed), whereas single CCSs from siRNA-moesin2-treated cells mainly moved in lateral trajectories from 1 μm to <6 μm (79% of analyzed CCSs) (supplemental Fig. S1*C*). Therefore, the average area of movement for the analyzed CCSs showed the following values for the trajectory radius: 0.7 ± 0.084 μm in control (scrambled) cells and 1.4 ± 0.142 μm in moesin-silenced cells (Fig. 2*E*). Therefore, the results obtained were not conditioned by the siRNA oligonucleotide used to interfere with moesin protein expression, and depended on the specific silencing of the endogenous moesin protein.

We also observed an unusual aggregation of single LCa-DsRed-labeled CCSs in moesin-silenced cells in the evanescent field (Fig. 2*C*, *white arrowheads*, and Fig. 2*G*, see representative *clusters 1* and *2*). These clusters of CCSs were also observed in cells lacking moesin after treatment with the siRNA-moesin2 oligonucleotide (supplemental Fig. S1*B*). It appears that LCa-DsRed-labeled clusters are not formed by abnormal fusion of CCSs, because they progressively dissociate in single LCa-DsRed-labeled structures (Fig. 2*G*, time-lapse of frames and line-scan analysis, and supplemental Movie S3, disaggregation of *cluster 1*). Fluorescence intensities of these sorted CCSs rapidly dimmed in the evanescent field suggesting that these CCSs either moved out from the evanescent field or lost the clathrin coat (supplemental Movie S3).

Therefore, we propose that the formation of these clusters may be due to the accumulation of individual CCVs that were not correctly trafficked in the absence of the F-actin-linker moesin (supplemental Movie S2 from moesin-silenced cells in Fig. 2*F*, tracked CCS joining aggregates of CCSs, at the *bottom* of the *movie*). These data indicate that moesin is a CCS linker that could regulate vesicle trafficking.

The N-terminal-PIP$_2$ Binding Domain of Moesin Mediates Its Co-distribution with CCSs—We performed TIRFM-based analysis of LCa-DsRed-labeled CCSs with different moesin-GFP constructs (22), expressed in HeLa cells (Fig. 3), to explore the structural features of moesin that are responsible for its co-distribution with CCSs. Three C-terminal GFP-tagged moesin constructs were used first: FL-moesin-GFP (full-length moesin), N-moesin-GFP (N-terminal domain), or C-moesin-GFP (the C-terminal actin binding region) (22). FL-moesin-GFP, which entirely conserves functional N-terminal and C-terminal F-actin-binding domains, anchors membrane structures to F-actin filaments. On the other hand, the N-moesin product, without the F-actin-binding domain, works as a dominant negative form by disconnecting endogenous moesin from both membrane structures and cortical actin. However, C-moesin protein product binds to F-actin filaments and lacks the ability to associate with membrane structures without any negative dominant effect on endogenous moesin (22).

We observed that overexpressed FL- and N-moesin-GFP molecules mainly distributed on plasma membrane-associated structures and also showed some diffuse intracellular distribution and a punctated expression pattern (Fig. 3, *A* and *B*), as described (22, 41). Hence, FL- or N-moesin-GFP molecules that presented a punctated pattern of expression co-distributed with LCa-DsRed-labeled CCSs (Fig. 3, *A* and *B*, *white arrows*, and quantified in Fig.
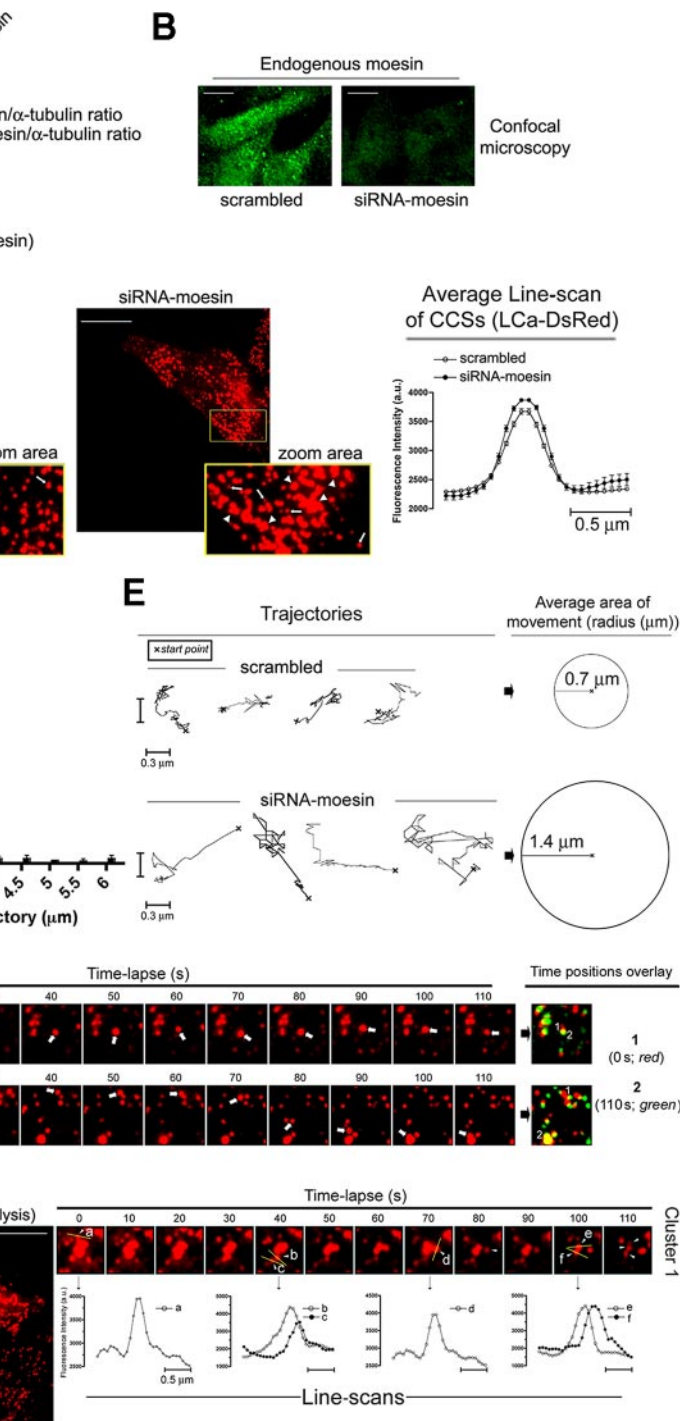
3*E*). However, the C-moesin-GFP protein product, which binds to F-actin (supplemental Fig. S4*C*, C-moesin-GFP and related *images*), presented a diffused expression pattern and did not co-distribute with LCa-DsRed-labeled CCSs as observed in the evanescent field (Fig. 3, *C* and *E*).

On the other hand, we observed certain aggregates of LCa-DsRed-labeled CCSs in cell regions where the dominant negative N-moesin-GFP molecule co-distributed (Fig. 3*B*, see *white arrowheads*). These clusters of CCSs were similar to those which appeared in moesin-silenced cells (Fig. 2*C*, see *white arrowheads* in the *siRNA-moesin image*, Fig. 2*G*, and supplemental Movie S3).

It is thought that the dominant negative effect exerted by the N-moesin construct, which anchors to membrane structures, lies in its capacity to bind to the C-terminal half of the endogenous moesin molecule, thereby disconnecting moesin from actin cytoskeleton (22). Therefore, N-moesin-GFP could alter the cellular distribution of CCSs by disrupting the anchoring of moesin-associated CCSs to F-actin, as was observed in moesin-silenced cells (Fig. 2). Thus, it appears that the N-terminal part of moesin is responsible for its co-distribution with CCSs, while the C-terminal part of moesin would help to link moesin-bearing CCSs to F-actin. FL-moesin-GFP molecules distributed with preformed LCa-DsRed-labeled CCSs on plasma membrane, and their associated fluorescence intensities rapidly dimmed together in the evanescent field (supplemental Fig. S2, *A* and *B*, respectively). These data indicate that FL-moesin-GFP/LCa-DsRed-labeled CCSs moved out in the *z* axis direction, which could represent nascent moesin-positive CCVs.

The term "endocytic adaptor" is generally reserved for proteins that bind to PIP_2 and also to clathrin, both of which are present in the CCSs (1). These adaptors affect the cargo-induced sorting signals during endocytosis, by interacting with the cytoplasmic tails of the CCV-associated cargos (1). The moesin protein, like other F-actin-linkers from the ERM family, presents the $KK(X)_n(K/R)K$ consensus binding site for PIP_2 at the N-terminal part of the molecule (42). More-

over, PIP_2 is required for the conformational activation of ERM proteins (43, 44). Therefore, we studied whether moesin associates to CCSs through its consensus PIP_2-binding domain. Combined K/N mutations of the Lys residues 253 and 254, and 262 and 263, are responsible for the loss of the interaction of ERM mutants with PIP_2 (16, 45). A similar effect is achieved in ezrin by combining the double mutation of residues K63N and K64N with the double K253N,K254N mutation (45). Then, the mutation of four N-terminal Lys residues, within the $KK(X)_n(K/R)K$ motifs, eliminates the

capacity of ERM proteins to bind to PIP$_2$, which redistribute to the cytoplasm (16, 45).

Therefore, and based on previous inactivating mutations reported for ezrin (16, 45), we have created a new construct by changing the N-terminal Lys residues 253, 254, 262, and 263 into Asn, thereby generating the K253N,K254N,K262N,K263N-moesin-GFP (4K/4N-moesin-GFP) mutant (Fig. 3D). As compared with the FL-moesin-GFP molecule (Fig. 3, A and F, and supplemental Fig. S3A), the inert 4K/4N-moesin-GFP mutant mainly presented a diffused and altered cytoplasmic distribution (Fig. 3D), which did not bind soluble PIP$_2$ (Fig. 3F) and did not distribute to PIP$_2$-enriched plasma membrane domains (supplemental Fig. S3B), as monitored by the fused ECFP-tagged pleckstrin homology domain of the phosphatidylinositol-specific phospholipase Cδ_1 (ECFP-PH) (23–25). In fact, the 4K/4N-moesin-GFP molecule no longer co-localized with LCa-DsRed-labeled CCSs, and mainly presented a cellular distribution pattern similar to the C-moesin-GFP construct (Fig. 3D, TIRFM images, and quantified in Fig. 3E). This inert mutant did not have any effect on the distribution and organization of LCa-DsRed-labeled CCSs (Fig. 3D).

Moreover, moesin knockdown (supplemental Fig. S4, A and B) or overexpression of FL-moesin-GFP or 4K/4N-moesin-GFP molecules (supplemental Fig. S4C) affected neither cell morphology nor actin cytoskeleton. Therefore, we propose that the N-terminal-PIP$_2$-binding domain of moesin is responsible for its co-distribution with the different CCSs, and that the moesin molecules associated with CCSs could be involved in the trafficking of nascent endocytic CCVs.

Moesin Is Involved in the Trafficking of Nascent rab5-CCVs— We tracked LCa-DsRed-labeled CCSs in cells overexpressing fluorescent rab5 (Fig. 4), rab7, or rab11 (supplemental Fig. S5, A or B, respectively) small GTPases to analyze whether moesin silencing-mediated effects on the motility of CCSs occurred at a particular endocytic intermediate. These rab GTPases are considered to be specific markers for early endosomes, late endosomes, or for perinuclear vesicles that recycle from Golgi to plasma membrane, respectively (46, 47). We used fluorescent scrambled or siRNA-moesin oligonucleotides to identify, by epifluorescence, both intact control cells and cells without endogenous moesin (Fig. 4, A and B, respectively). We further analyzed, by TIRFM, the cellular distribution of the different rab GTPases under this experimental condition. Fluorescent

siRNA-moesin or -moesin2 oligonucleotides specifically silenced the expression of the endogenous moesin protein (Fig. 4E and supplemental Fig. S1A, *moesin Western blot bands*), and provoked an altered accumulation and aggregation of the CCSs, as observed in the evanescent field (Fig. 4B and supplemental Fig. S1B, *white arrowheads* indicate aggregates of CCSs).

We observed that moesin interference provoked the accumulation of ECFP-rab5/LCa-DsRed-labeled CCSs (Fig. 4C, *TIRFM images*, and quantified in Fig. 4D, ~30% of increase), when compared with control cells. The observed basal level of rab7- or rab11-labeled CCSs was not significantly affected in moesin-silenced cells (supplemental Fig. S5, A or B, respectively, and quantified in bar histograms). The transfected ECFP-rab5 protein was equally expressed in both control and moesin-silenced cells (Fig. 4E, ECFP-rab5 Western blot bands), as occurred with fluorescent rab7 and rab11 molecules (data not shown). Furthermore, the overexpressed amount of ECFP-rab5 did not alter the cell-surface expression level of TfR and did not affect the uptake of the Tf ligand (Fig. 4, F and G, respectively). Hence, it seems that CCSs were not perturbed by the overexpressed amount of the ECFP-rab5 molecule. Taking all these data together, we suggest that moesin knockdown induces the accumulation of CCSs carrying the rab5 molecule.

Similar results were obtained in moesin-silenced cells overexpressing the ECFP-rab5, LCa-DsRed, and GFP-α-adaptin molecules (Fig. 5A). First of all, we observed that LCa-DsRed and GFP-α-adaptin molecules showed a high degree of co-distribution (Fig. 5A, and quantified in Fig. 5B) indicating that the LCa-DsRed-labeled structures could be considered as functional CCSs, as previously described (48–51). Moreover, specific moesin knockdown provoked the increase of ECFP-rab5/GFP-α-adaptin/LCa-DsRed-colabeled structures in intact moesin-silenced cells (Fig. 5A, and quantified in Fig. 5C). The ECFP-rab5 molecule was equally expressed both in control and moesin-silenced cells (Fig. 5A, and quantified in Fig. 5D, Western blot). We propose that these accumulated structures represent nascent endocytic CCVs, containing the rab5 GTPase, as was further confirmed by comparative studies on plasma-membrane sheets (Fig. 5E).

Plasma-membrane sheets were prepared from scrambled (control) or moesin-silenced cells, expressing ECFP-rab5, TfR-EGFP, and LCa-DsRed molecules (Fig. 5E). It is worth mentioning that the basal level of co-distribution of TfR-EGFP/ECFP-

FIGURE 2. **Silencing of endogenous moesin alters normal trafficking of CCSs and provokes their clustering.** *A*, Western blot analysis of specific moesin knockdown (siRNA-moesin) in HeLa cells compared with control (scrambled) cells. Silencing of endogenous moesin is quantified as the ratio of moesin and α-tubulin band intensities, compared with the values for ezrin molecule. A representative experiment of three is shown. *B*, confocal microscopy images (maximal projections) for endogenous moesin silencing (siRNA-moesin), compared with control (scrambled) HeLa cells. *C*, TIRFM analysis of LCa-DsRed-associated CCSs in scrambled or moesin-silenced (siRNA-moesin) HeLa cells. In the *zoom area* of scrambled or moesin-silenced (siRNA-moesin), CCSs (<0.5 μm; see "Experimental Procedures") are indicated by *white arrows*. *Right*, average CCS-diameter size for CCSs, analyzed by line scan, under any experimental condition. Data are mean ± S.E. (n = 200 CCSs from six different cells). *White arrowheads* indicate abnormal clustering of LCa-DsRed-labeled CCSs in the *zoom area* of moesin-silenced (siRNA-moesin) cells. *D*, analysis of the movement (radius of the trajectories) of LCa-DsRed-labeled CCSs in control (scrambled) or moesin-silenced (siRNA-moesin) HeLa cells. Data are from 120 CCSs counted in 10 different cells per experimental condition. *E, left*, four different and representative movement trajectories for LCa-DsRed-labeled CCSs are shown for control (scrambled) or moesin-silenced (siRNA-moesin) cells. The *x* symbol indicates the starting point for each trajectory indicated. *Right*, average area of movement for CCSs in cells without moesin (siRNA-moesin), compared with control cells (scrambled). The *average radius* indicates the maximum trajectories observed, under any experimental condition. Data are mean ± S.E. from three independent experiments: in each experiment, 120 CCSs were counted in 10 different cells per experimental condition. *F*, TIRFM-based time-lapse study of CCS movement for 110 s, in control (scrambled) or moesin-silenced (siRNA-moesin) HeLa cells (see *white arrow-labeled vesicles*). The *time position overlay panel* shows initial (0 s, *red*) and final (110 s, *green*) positions (*1* and *2*, respectively) for the tracked CCSs, in the same image. *G*, time-lapse analysis of the decay of the fluorescence intensity of single CCSs sorted from CCS aggregates, observed in the evanescent field of moesin-silenced cells. *Line scans* show the fluorescent intensity profiles for any of the sorted individual CCSs (*cluster 1* from the *cellular square area*), indicated with *a–f* symbols, and analyzed at times 0 s, 40 s, 70 s, and 100 s, respectively. *Bar*, 10 μm.
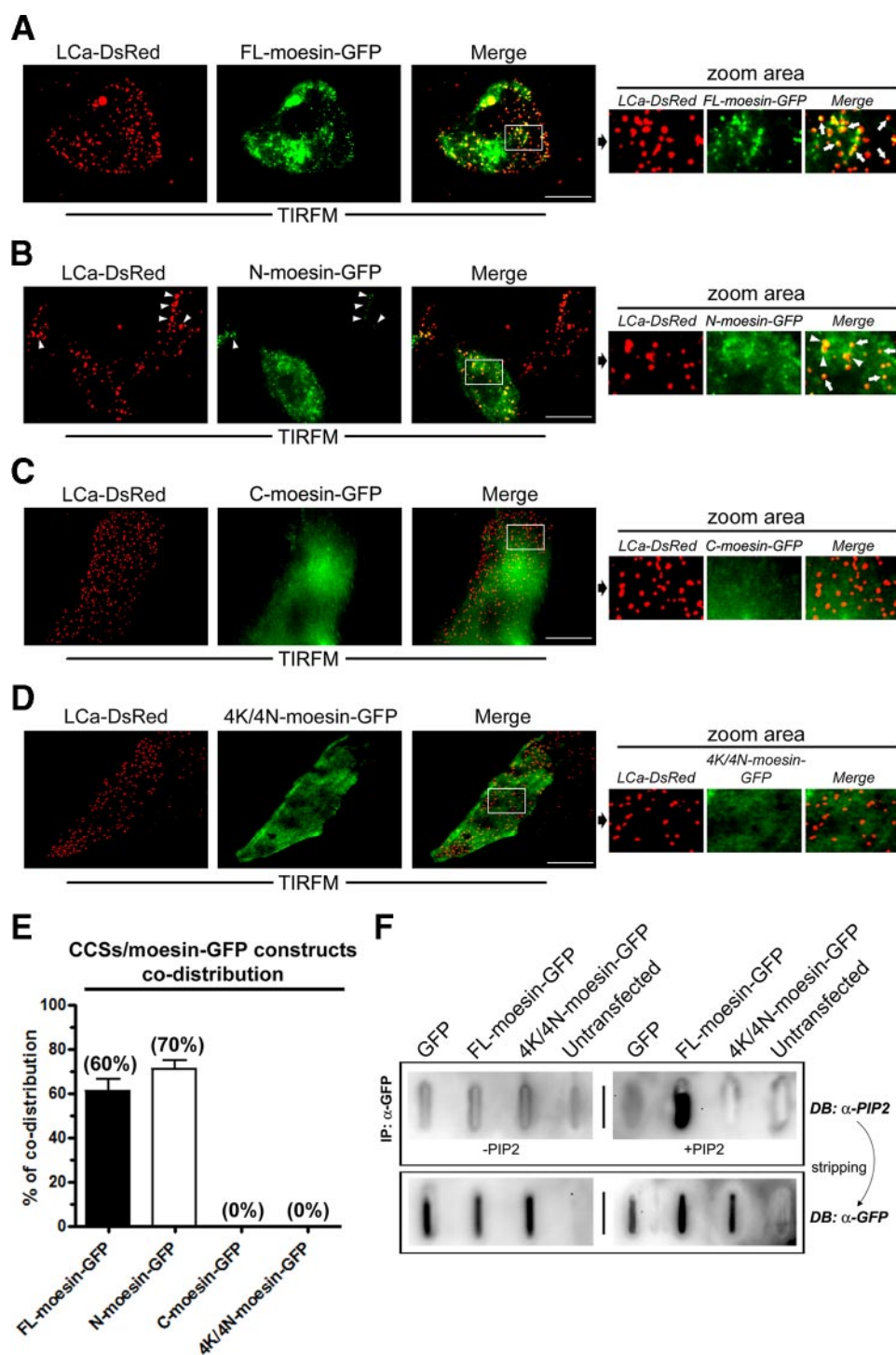
FIGURE 3. The PIP$_2$-binding domain of moesin is responsible for its association with CCSs. *A–D*, TIRFM images for the analysis of co-distribution of LCa-DsRed-labeled CCSs with FL-, N-, C-, or 4K/4N-moesin-GFP constructs, respectively, in HeLa cells. In the *zoom areas*, *white arrows* indicate representative CCS, where LCa-DsRed molecules co-distributed with FL- or N-moesin-GFP products, whereas *white arrowheads* indicate abnormal clustering of LCa-DsRed-labeled CCS co-distributed with N-moesin-GFP. *Bar*, 10 μm. *E*, bar histograms show the quantification of the co-distribution of FL-, N-, C-, and 4K/4N-moesin-GFP molecules with LCa-DsRed-labeled CCSs. Data are mean $\pm$ S.E. ($n = 500$ spots from 5 different cells). The quantification was performed as described under "Experimental Prodecures." *F*, *top dot blots*, dot-blot analysis of PIP$_2$ bound to purified FL-moesin-GFP and 4K/4N-moesin-GFP molecules (*DB*: α-PIP$_2$) from lysates of respective nucleofected cells, previously immunoprecipitated by using a specific antibody against GFP (*IP*: α-GFP). *Bottom dot blots*, dot-blot analysis of the presence of the nucleofected and immunoprecipitated GFP, FL-moesin-GFP, and 4K/4N-moesin-GFP molecules (*DB*: α-GFP), after membrane stripping of the *top dot blots*. This experiment was performed in lysates from cells nucleofected by GFP, FL-moesin-GFP, or 4K/4N-moesin-GFP, and compared with lysates from untransfected cells. A representative experiment of three performed experiments is shown.

rab5/LCa-DsRed-labeled structures did not change after moesin knockdown (Fig. 5*E*, ~10% of total observed CCSs, as shown in the *zoom areas*). These structures could correspond to deeply invaginated CCSs that have been described as containing the rab5 GTPase to promote the formation of functional transport vesicles (52). In fact, aggregates of ECFP-rab5/LCa-DsRed-labeled structures, shown in intact moesin-silenced cells (Figs. 4*C*, 6*B*, and 6*C*), were not detected in plasma-membrane sheets (Fig. 5*E*). Thereby, this indicated that these accumulated structures correspond to nascent endocytic rab5-CCVs (Figs. 4*C*, 6*B*, and 6*C*), which were removed during the cell rip-off (Fig. 5*E*). The majority of the CCSs detected in control or moesin-silenced plasma-membrane sheets were rab5-negative, and therefore represent CCPs. Patches of CCPs were not observed in moesin-silenced plasma-membrane sheets (Fig. 5*E*). These data support the fact that moesin knockdown affects cellular location and trafficking of nascent endocytic CCVs, but not CCP and CCV formation (or the TfR uptake process). Therefore, the impaired link of rab5-CCVs to F-actin filaments, after moesin silencing, perturbs the trafficking of these endocytic vesicles.

Moesin Silencing Provokes the Accumulation of TfR in Nascent rab5-CCVs, Affecting Its Cell-surface Expression and Recycling Process—TfR is constitutively associated to CCPs (8) and follows internalization, via CCVs, regardless of Tf-ligand engagement (53). Therefore, we studied the functional consequences of specific moesin knockdown in the accumulation of the TfR in nascent rab5-CCVs.

This is why we silenced endogenous moesin (Fig. 6*A*, *left Western blot panel*) in cells overexpressing TfR-EGFP, ECFP-rab5, and LCa-DsRed constructs (Fig. 6). The ECFP-rab5 molecule was equally overexpressed both in moesin-silenced and scrambled-control cells (Fig. 6*A*, *right Western blot panel*).
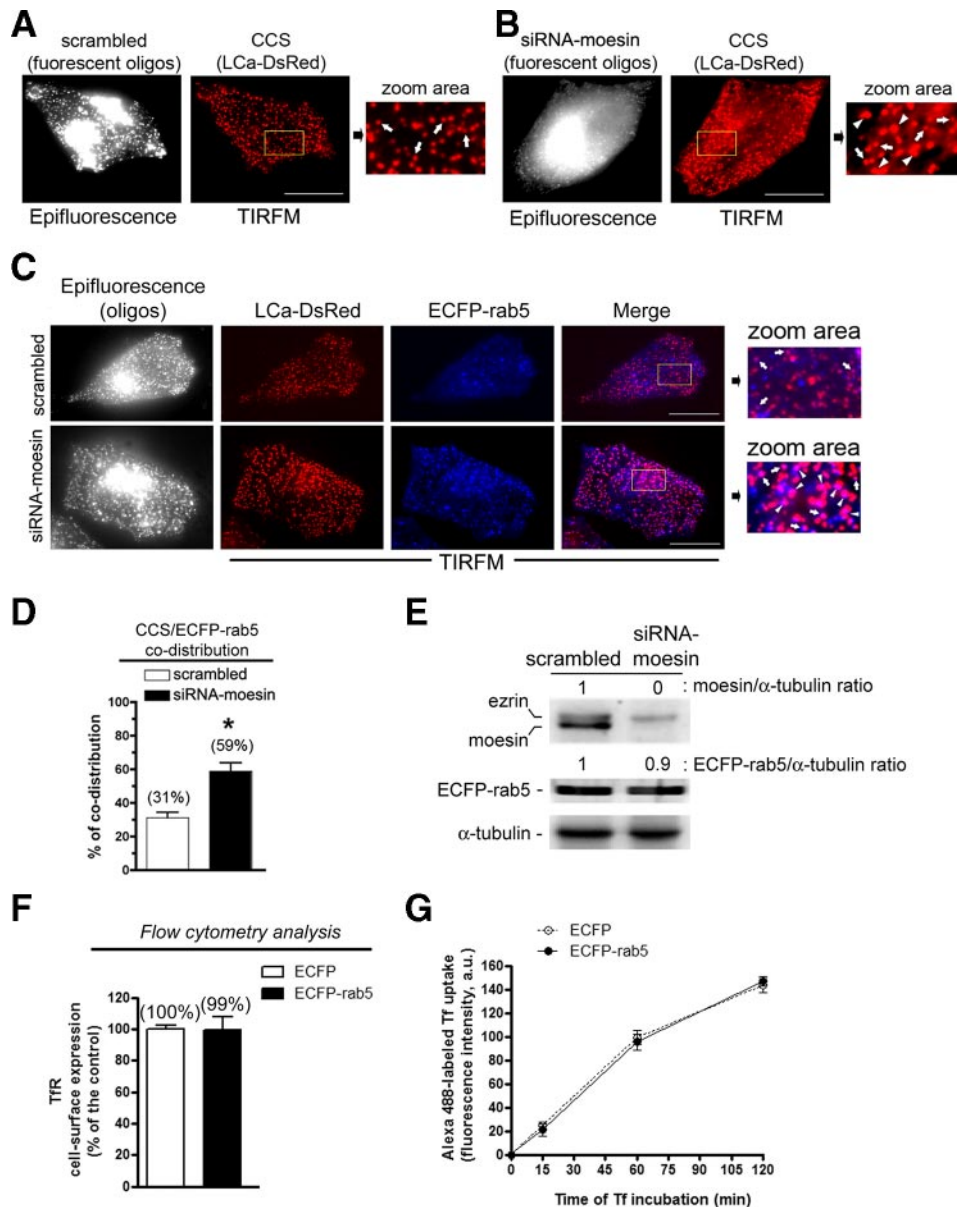
FIGURE 4. **Silencing of endogenous moesin provokes the accumulation of rab5-CCSs.** *A* and *B*, TIRFM analysis of LCa-labeled CCSs in HeLa cells treated with fluorescent-scrambled and siRNA-moesin oligonucleotides, monitored by epifluorescence. In the *zoom area*, *white arrows* indicate single representative CCSs (<0.5 μm, see "Experimental Procedures"), whereas *white arrowheads* indicate clusters of CCSs (*siRNA-moesin panel*). *C*, moesin silencing effect on LCa-DsRed-labeled CCSs in HeLa cells overexpressing ECFP-rab5, compared with control cells (scrambled). In the *zoom area*, *white arrows* indicate CCSs carrying the fluorescent rab5 marker, under any experimental condition. *White arrowheads* indicate clusters of CCSs in the *zoom area* of siRNA-moesin cells. *D*, *bar histograms* show the percentage of ECFP-rab5/LCa-DsRed co-distribution. Data indicated in *bar histograms* are mean ± S.E. (*n* = 1000 spots from 5 different cells). *, *p* < 0.05, *t* test. *E*, Western blot analysis of ECFP-rab5 expression and moesin knock-down, by using fluorescence siRNA-moesin oligonucleotides, compared with fluorescent control (scrambled) oligonucleotides. Silencing of endogenous moesin is quantified as the ratio of moesin and α-tubulin band intensities, under any experimental condition, and compared with the ezrin molecule. The total level of expression of the transfected ECFP-rab5 molecule was quantified as the ratio of ECFP-rab5 and α-tubulin band intensities, both in control and moesin-silenced cells. A representative experiment is shown. *F*, flow cytometry analysis for the quantification of TfR (CD71) cell-surface expression in control cells (overexpressing the ECFP protein, *open histograms*) or cells overexpressing the ECFP-rab5 small GTPase (*solid histograms*) cells. Data were corrected by subtracting the nonspecific adsorption of antibodies, determined by using an IgG-isotype negative control. Data are mean ± S.E. (*n* = 9, from three independent experiments). *G*, Alexa 488-labeled Tf uptake, determined at 15 min, 1 h, and 2 h, and analyzed by flow cytometry, in control (overexpressing the ECFP protein) or cells overexpressing the ECFP-rab5 molecule. Data are mean ± S.E. (*n* = 9, from three independent experiments). In *A–C* the presence of the fluorescent scrambled or siRNA-moesin oligonucleotides is monitored by epifluorescence. *Bar*, 10 μm.

Cells without endogenous moesin accumulated endocytic rab5-CCVs, as monitored by ECFP-rab5/LCa-DsRed co-distribution (Fig. 6, *B* and *C*, and quantified in Fig. 6*D*). The specific

silencing of moesin did not alter the constitutive association of TfR with CCSs (Fig. 6, *B–E*, and quantified in Fig. 6*F*). Furthermore, it was observed that the TfR-EGFP, ECFP-rab5, and LCa-DsRed molecules co-distributed in these nascent CCVs (rab5-CCVs), in scrambled and in moesin-silenced cells (Fig. 6*E*). However, only moesin knockdown favors the retention of the TfR in rab5-CCVs as was detected by an increase in the TfR-EGFP/ECFP-rab5/LCa-DsRed structures (Fig. 6*B*, *siRNA-moesin images*, and quantified in Fig. 6*D*). It is conceivable that these altered endocytic rab5-CCVs containing the TfR may represent, in part, a compartment of clathrin-containing endosomes that have been previously described as being highly motile and as accumulating the Tf ligand (50).

Flow cytometry analysis of moesin-silenced cells showed reduced expression levels of the TfR at the cell surface (Fig. 7*A*, ~40% reduction), when compared with control (scrambled) cells. We then examined the ability of these cells to uptake Alexa 488-labeled Tf ligand (see "Experimental Procedures"). We observed that the rate of early internalization of Tf was similar in control and moesin-silenced cells (Fig. 7*B*), indicating that moesin did not affect Tf uptake. Therefore, the reduced cell-surface expression of TfR, in cells lacking moesin, could be due to its retention in the altered nascent rab5-CCVs rather than a defect in TfR internalization.

We analyzed the endosomal distribution of endogenous TfR, by a biochemical approach in moesin-silenced cells, and compared this to control (scrambled) cells (Fig. 7, *C* and *D*) to further confirm that moesin knockdown provokes the accumulation of the TfR in endocytic rab5-CCVs. To do this, we centrifuged postnuclear supernatants of moesin-silenced or control (scrambled) cells, on shallower 5–20% Optiprep™ gradients (see "Experimental Procedures"), and the distributions of moesin, ezrin, TfR, rab5, and rab7 proteins were determined in each subcellular fraction collected by Western blot and by using specific anti-
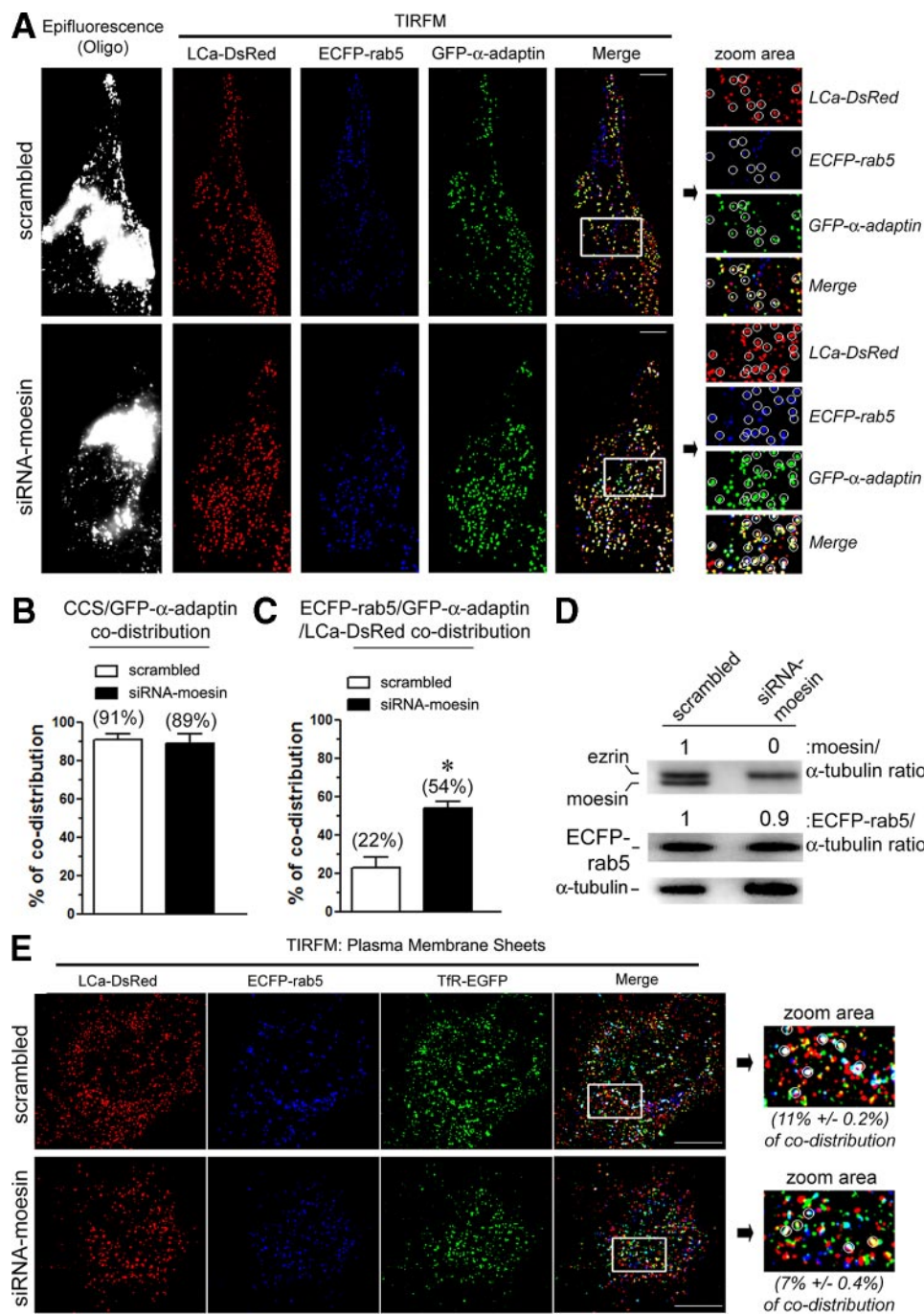
FIGURE 5. **Moesin knockdown provokes the accumulation of nascent rab5-CCVs.** *A*, moesin silencing effect on cellular distribution of ECFP-rab5/GFP-α-adaptin/LCa-DsRed-labeled CCSs, compared with control cells (scrambled). Accumulated rab5-CCSs were monitored by the ECFP-rab5/GFP-α-adaptin/LCa-DsRed labeling (*Merge images*). The presence of the fluorescent scrambled or siRNA-moesin oligonucleotides is monitored by epifluorescence. *Zoom areas*, *circles* in scrambled and siRNA-moesin cells indicate ECFP-rab5/LCa-DsRed-CCSs co-distributing with the GFP-α-adaptin molecule. *Bar*, 5 μm. *B*, *bar histograms* show the quantification of LCa-DsRed/GFP-α-adaptin co-distribution in scrambled (control cells) and in moesin-silenced cells (*open* and *solid histograms*, respectively). *C*, *bar histograms* show the quantification of ECFP-rab5/LCa-DsRed/GFP-α-adaptin co-distribution in scrambled (control cells) and in moesin-silenced cells (*open* and *solid histograms*, respectively). *, $p < 0.05$, *t* test. Data in *B* and *C* are mean ± S.E. ($n = 500$ spots from 5 different cells). *D*, Western blot analysis of ECFP-rab5 expression and specific moesin knockdown (siRNA-moesin) in HeLa cells, compared with control cells (scrambled), used to prepare plasma-membrane sheets. ECFP-rab5 expression or silencing of endogenous moesin is quantified as the ratio of ECFP-rab5/or moesin/α-tubulin band intensities. A representative experiment is shown. *E*, moesin silencing effect on LCa-DsRed, ECFP-rab5, and TfR-EGFP localization and co-distribution in plasma-membrane sheets, compared with scrambled (control) sheets. *Zoom areas*, *circles* indicate TfR-EGFP/ECFP-rab5/LCa-DsRed-colabeled structures (deeply invaginated rab5-CCSs), under any experimental condition. In the *zoom areas*, the percentages indicate the quantification of TfR-EGFP/ECFP-rab5/LCa-DsRed-colabeled structures observed in scrambled (control) or moesin-silenced plasma-membrane sheets. Data are mean ± S.E. ($n = 1000$ spots from 5 different preparations of plasma membrane sheets). *Bar*, 5 μm.

bodies against each molecule. The equilibrium distribution of the TfR, in scrambled (control) cells, was probed in the different fractions collected (Fig. 7*C*, *TfR line*). The rab5- and rab7-positive fractions were separated along the collected fractions, observing rab5 in the lower density fractions and rab7 in the densest fractions of the Optiprep™ gradient (Fig. 7*C*, *rab5* and *rab7 lines*). Endogenous moesin and ezrin were homogeneously detected in the isolated cellular compartments from scrambled cells (Fig. 7*C*, *ezrin/moesin line*). This observation confirms the above data obtained by TIRFM and confocal microscopy techniques, indicating that a part of the cellular pool of moesin co-distributed with CCSs. In contrast, only ezrin was detected along the endosome fractions collected in moesin-silenced cells (Fig. 7*D*). Indeed, the TfR mainly concentrates in the lowest density fractions together with the rab5 molecule (Fig. 7*D*, *TfR* and *rab5 lines*). Hence, moesin knockdown provoked the accumulation of endogenous TfR in rab5-positive low density fractions, which could correspond to an accumulation of rab5-CCVs carrying the TfR as observed by TIRFM (Figs. 5 and 6). Rab7 distribution, a marker for the late endosomes, did not appear to be altered by the specific silencing of moesin, in the Optiprep™ gradients, when compared with scrambled cells (Fig. 7, *C* and *D*, *rab7 lines*).

We measured the amount of Tf sequestered in control and moesin-silenced cells (Fig. 7*E*), to corroborate that moesin knockdown affects Tf recycling. To do this, cells were previously loaded with fluorescent Alexa 488-labeled Tf at 37 °C for 30 min. Cells were placed on ice and washed with acidic buffer to remove recycled surface-Tf. Cells were then shifted again to 37 °C to allow the recycling of the internalized Tf ligand, which was measured for the indicate time points. We observed that moesin-silenced cells exhibited a low rate of Tf recycling when compared with the rate of Tf released in
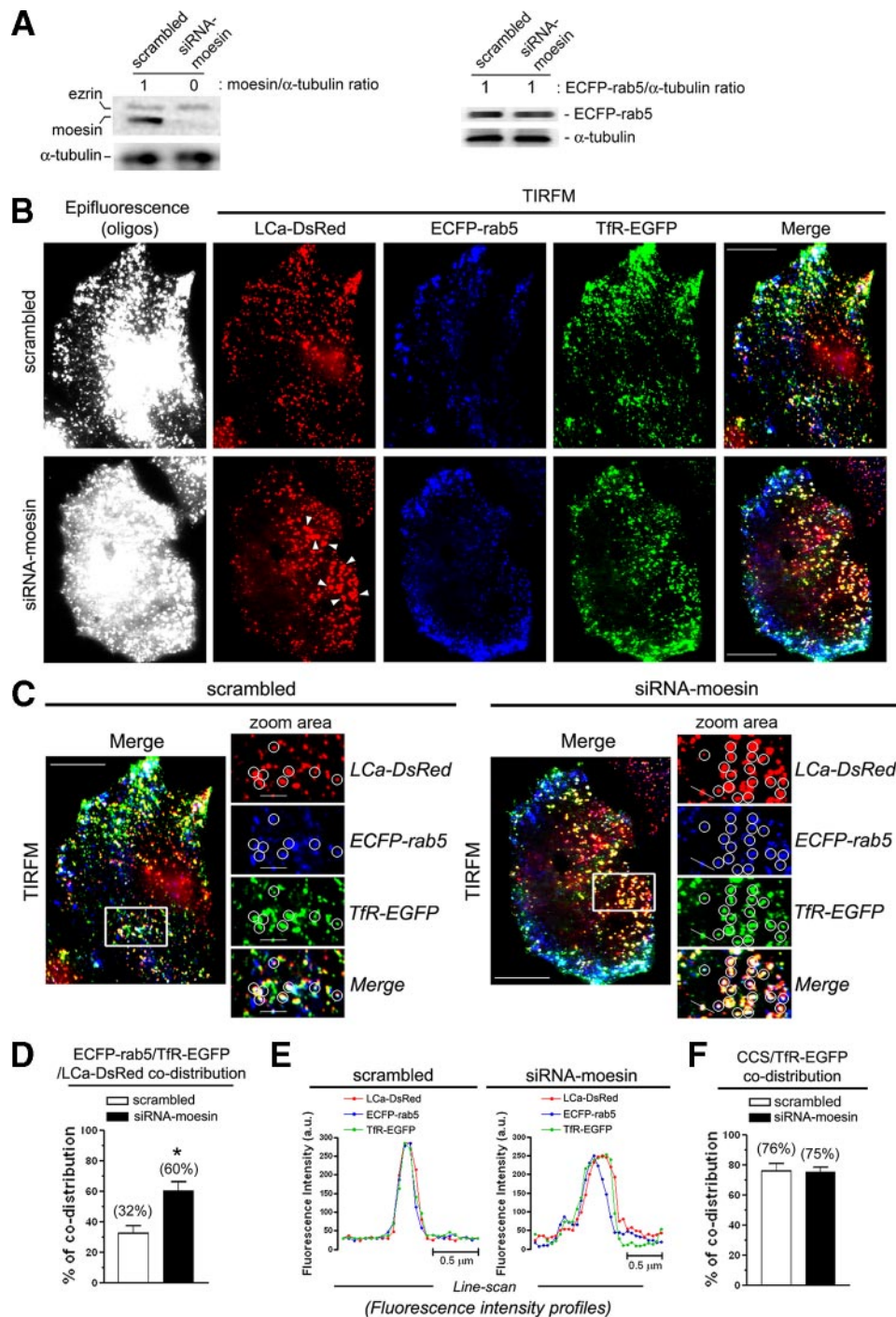
A, Western blot analysis of specific moesin knockdown (siRNA-Moesin) (*left panel*), or overexpression of the ECFP-rab5 molecule (*right panel*), in moesin-silenced cells compared with control cells (scrambled). Silencing of endogenous moesin or expression of the ECFP-rab5 molecule is quantified as the ratio of moesin/or ECFP-rab5/α-tubulin band intensities. A representative experiment of three performed experiments is shown. *B* and *C*, moesin silencing effect on cellular distribution and trafficking of the TfR-EGFP, constitutively associated to LCa-DsRed-labeled CCVs, compared with control cells (scrambled). The accumulation (important in moesin-silenced cells) of the TfR-EGFP, in nascent rab5-CCVs, was monitored by ECFP-rab5/LCa-DsRed-CCVs/TfR-EGFP co-labeling (*Merge images* in *B* and *C*). The presence of the fluorescent scrambled or siRNA-moesin oligonucleotides is monitored by epifluorescence. The *white arrowheads* indicate clusters of LCa-DsRed-labeled CCVs in siRNA-moesin cells (*B*). In *C*, circles in scrambled and siRNA-moesin cells indicate ECFP-rab5/LCa-DsRed-labeled CCVs carrying the TfR-EGFP (nascent rab5-CCVs). *Bar*, 8 μm. *D*, *bar histograms* show the accumulation percentage of nascent ECFP-rab5/LCa-DsRed-labeled CCVs carrying the TfR-EGFP receptor. *, *p* < 0.05, *t* test. Data in *D* and *F* are mean ± S.E. (*n* = 500 spots from 5 different cells). *E*, line-scan analysis of LCa-DsRed, ECFP-rab5, and TfR-EGFP co-distribution in representative single nascent rab5-CCV of scrambled and moesin-silenced cells, indicated by the *line* in the *zoom areas* of *C*. *F*, *bar histograms* show the percentage of TfR-EGFP/LCa-DsRed co-distribution in scrambled (control) and moesin-silenced (siRNA-moesin) cells.

FIGURE 6. **Moesin knockdown provokes accumulation of the TfR in nascent endocytic-CCVs.**

control (scrambled) cells (Fig. 7*E*). These observations could indicate a normal recycling process in control cells, which released the Tf ligand, as well as an altered process in moesin-silenced cells that retained the intracellular Tf.

On the other hand, we observed by TIRFM that the exocytosis of TfR-phl to the plasma membrane occurred with a similar frequency, both in control (scrambled) and moesin-silenced cells (Fig. 7*F*, and supplemental Movie S4). Interestingly, endogenous moesin slightly co-distributed with γ-adaptin (AP-1) (Fig. 1*C*), and moesin knockdown did not affect the number of rab11-positive CCSs detected at plasma membrane, when compared with control (scrambled) cells (supplemental Fig. S5*B*). Therefore, it seems that moesin is not involved in the *trans*-Golgi network-endosome transport and/or sorting of the TfR to the plasma membrane.

Moreover, we analyzed by TIRFM the association between the cell-surface expression level of TfR-phl and the amount of LCa-DsRed expressed per single CCS in control (scrambled) and moesin-silenced cells (Fig. 8*A*, *top histograms*). The TfR-phl molecule is a fusion construct with superecliptic phluorin attached to the extracellular domain of TfR. This phluorin molecule is a pH-sensitive variant of GFP in which fluorescence is almost completely quenched on transition from pH 7.4 to pH 5.5 (54, 55). Hence, it is thought that the TfR-phl fluorescence observed by TIRFM corresponds to TfR-phl molecules at the cell-surface associated wth CCPs or with non-endocytic CCSs (8, 56).

We observed, under this experimental condition that the average level of expression of the LCa-DsRed molecule per analyzed spot (TfR-phl/CCS) was not altered after moesin knockdown, when compared with control cells (Fig. 8*A*, *left histograms*). The fluorescence intensities of clathrin (LCa-DsRed) and TfR-phl in any analyzed CCS are proportional, which shows that CCS size influences the amount
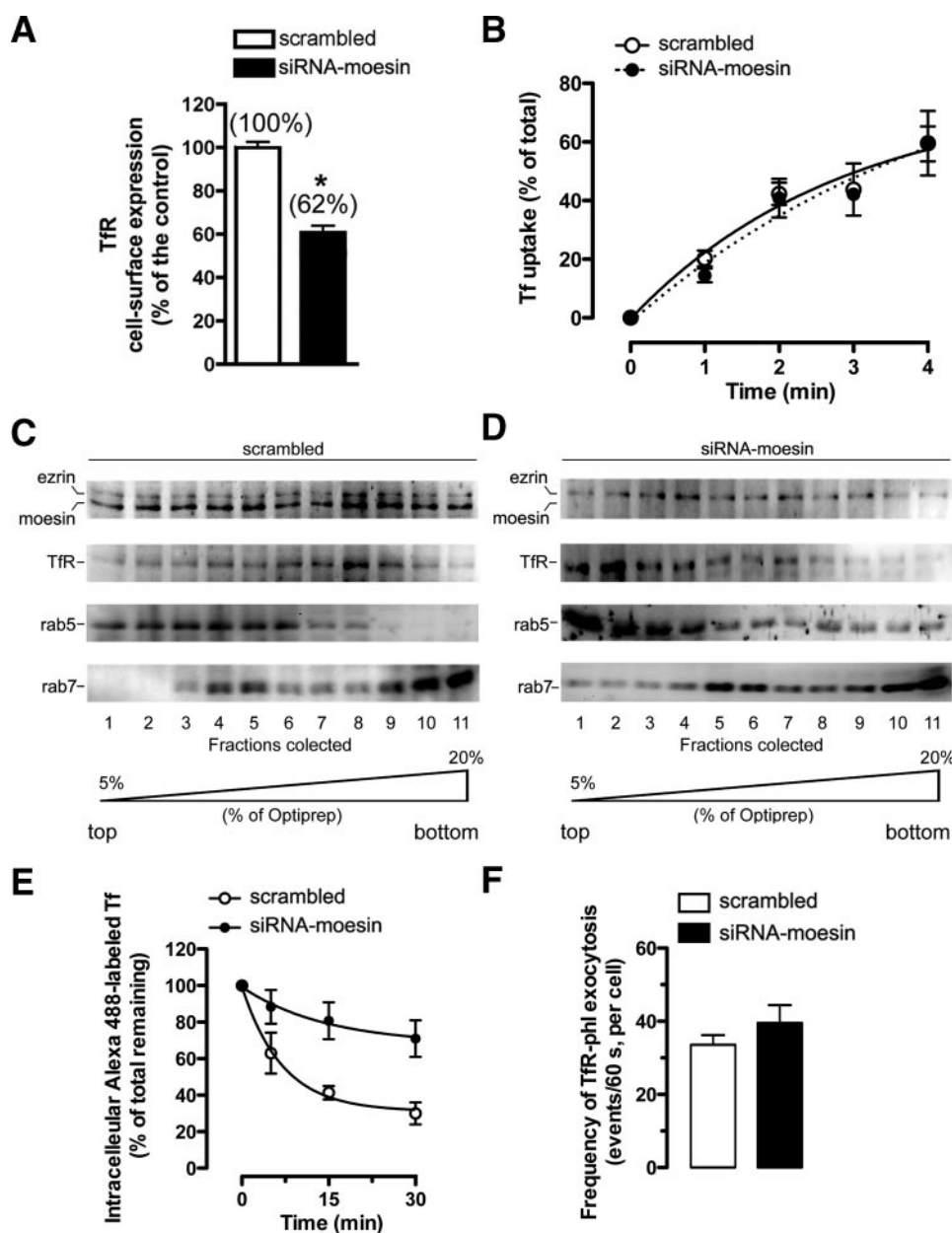
FIGURE 7. **Moesin knockdown perturbs TfR recycling, affecting TfR cell-surface expression.** *A, bar histograms* indicate specific TfR (CD71) cell-surface expression in control (scrambled) or moesin-silenced (siRNA-moesin) cells quantified by flow cytometry. Data were corrected by subtracting the nonspecific adsorption of antibodies, determined by using an IgG-isotype negative control. Data are mean ± S.E. (*n* = 6, from three independent experiments). *, *p* < 0.05, *t* test. *B*, early Tf uptake of Alexa 488-labeled Tf determined by flow cytometry in control (scrambled) or moesin-silenced (siRNA-moesin) cells for the indicated time points. Results are expressed as the percentage of internalized Tf with respect to the total prebound Tf ligand at +4 °C (100%), in each experimental condition. Data are mean ± S.E. (*n* = 9, from three independent experiments). *C* and *D*, Western blot analysis of the distribution of TfR, ezrin, and moesin molecules along the endosome, rab5-positive, and rab7-positive fractions collected (*1–11*, from *top* to *bottom*), obtained by Optiprep™ density gradient (5–20%) of cell lysates from scrambled (control) or moesin-silenced (siRNA-moesin) HeLa cells (*C* or *D panels*, respectively). Data are a representative experiment of three. *E*, quantification of Alexa 488-labeled Tf sequestered in control (scrambled) or moesin-silenced (siRNA-moesin) cells, determined by flow cytometry for the indicated time points. Results are expressed as the percentage of initial (time 0, 100%) intracellular Tf that was detected in cells during reincubation (see "Experimental Procedures"), in each experimental condition. Data are mean ± S.E. (*n* = 6, from three independent experiments). *F*, quantification of the TfR-phl frenquency of exocytosis in control (scrambled) and moesin-silenced cells (see supplemental Movie S4 for representative sequences of TfR-phl exocytosis monitored by TIRFM, in control and moesin-silenced cells). Data in the *histograms* are mean ± S.E. (*n* = 12 individual cells analyzed, from three independent experiments, under any experimental condition).

in the plasma membrane (Fig. 8*A*, *TIRFM images*). To quantify the level of expression of TfR-phl on the cell surface, under any experimental condition, we identified isolated CCSs and measured the fluorescence intensities for both LCa-DsRed and TfR-phl (Fig. 8*A*, see *zoom squares* in *TIRFM images*), as described under "Experimental Procedures." Bearing in mind that the LCa-DsRed expression is not affected after moesin knockdown (Fig. 8*A*, *left histograms* and *images*), the average ratio of TfR-phl/LCa-DsRed-associated fluorescence intensities, per analyzed spot (CCP), is indicative of the expression level of TfR-phl on the cell surface, under any experimental condition. We observed that cells lacking moesin presented a reduced TfR-phl expression at the cell surface (~51%), when compared with control cells (Fig. 8*A*, *right histograms*).
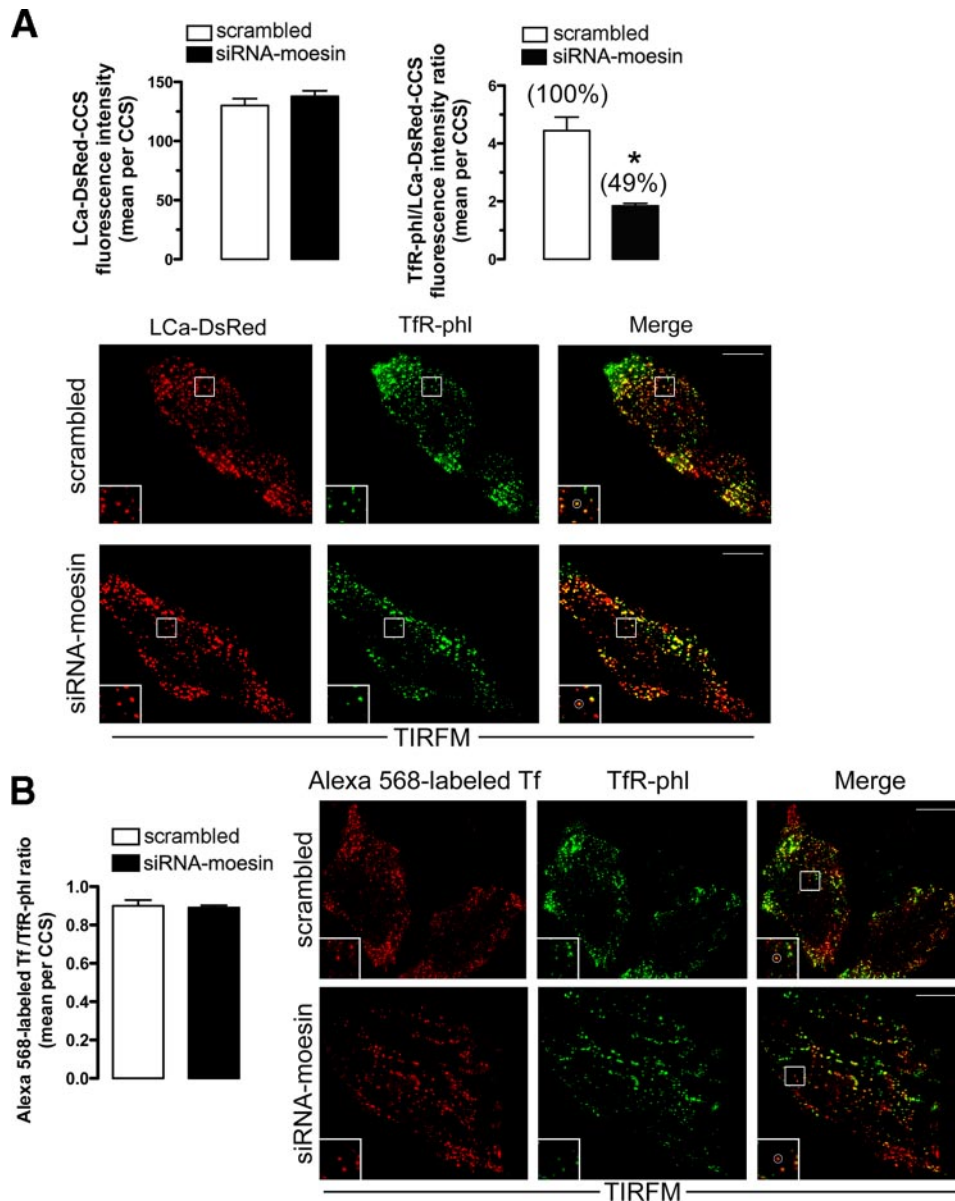
Furthermore, we observed that the Alexa 568-labeled Tf ligand was able to bind to TfR-phl at the cell surface, both in control and moesin-silenced cells (Fig. 8*B*, *TIRFM images*). To measure the Tf/TfR association at the cell surface, under any experimental condition, we identified isolated TfR-phl spots and measured the fluorescence intensities for both bound Alexa 568-labeled Tf and TfR-phl (see "Experimental Procedures"). The average fluorescence intensity Alexa 568-labeled Tf/TfR-phl ratios, per analyzed spot, were similar in the control and cells lacking moesin (Fig. 8*B*, *histograms*). Therefore, the reduced Tf uptake, observed after moesin knockdown (Fig. 7*B*), could be due to the reduced expression level of the TfR on the cell surface of moesin-silenced cells, as observed (Fig. 7*A*, *flow cytometry*, and Fig. 8*A*, *TIRFM*), and not to a change in the Tf/TfR binding ability or to an impaired TfR uptake. Taking all the

of the TfR-phl carried per structure, as previously described (8). Hence, it seems that moesin silencing did not affect CCP formation, and TfR-phl appeared to be concentrated in CCSs

above results together, we propose that moesin is key for driving the TfR recycling from endocytic rab5-CCVs to the plasma membrane.

FIGURE 8. **Moesin silencing diminished the average level of expression of TfR-phl per CCS, without affecting clathrin expression and Tf/TfR ligation.** *A*, *left bar histograms* indicate the average LCa-DsRed-associated fluorescence intensity per single CCS (spot) analyzed, as indicated in the *zoom square* of *TIRFM images*. *Right bar histograms* indicate the average TfR-phl/LCa-DsRed-associated fluorescence intensity ratio per single CCS analyzed, as indicated in the *zoom square* of *TIRFM images*. In both *histograms*, data are mean ± S.E. (*n* = 100 independent spots analyzed from 8 different control (scrambled) or moesin-silenced cells). *, *p* < 0.05, *t* test. Images of representative cells used to measure the level of expression of LCa-DsRed and TfR-phl per CCS (spot), at cell surface of control (scrambled) or moesin-silenced cells, are shown (see "Experimental Procedures"). *Encircled* spots in the *zoom squares* represent single analyzed TfR-phl/CCS. *Bar*, 10 μm. *B*, TIRFM analysis of the binding ability of Alexa 568-labeled Tf to cell-surface TfR-phl, in control and cells without moesin (see "Experimental Procedures"). *Bar histograms* indicate the average Alexa 568-labeled Tf/TfR-phl-associated fluorescence intensity ratios per analyzed TfR-phl-spot, as indicated in the *zoom squares* of representative cells, under any experimental condition. Data are mean ± S.E. (*n* = 100 independent spots analyzed from 8 different control (scrambled) or moesin-silenced cells). *Bar*, 10 μm.

DISCUSSION

In the present work, we describe the functional involvement of the F-actin linker moesin during CCV trafficking by acting on nascent rab5-CCVs. We observe that a part of the endogenous pool of moesin co-distributes with CHC and α-adaptin molecules, constitutive key components for CCS formation and related functions (29–33). The moesin silencing-mediated effect on LCa-DsRed-labeled CCSs motility and

cellular distribution suggests that moesin could be involved in the trafficking of CCVs. Lateral trajectories of CCSs were larger in moesin-silenced cells than those observed in control cells. In addition, silencing of moesin provokes the formation of CCS clusters, which progressively disaggregate into single structures. These events suggest that moesin may function as a regulatory linker for vesicle motility.

Because PIP_2 is required for the conformational activation of ERM proteins and mediates their association with F-actin (43, 44), it is plausible that moesin molecules, bound to the PIP_2 on nascent endocytic CCVs, are activated to anchor these vesicles to F-actin, thereby driving the trafficking process. However, we cannot rule out the possibility that moesin might also interact with other CCS-associated components other than PIP_2. PIP_2 facilitates the interaction of ERM with the cytoplasmic tails of several membrane proteins, such as CD43, CD44, ICAM-1, ICAM-2, and ICAM-3 (16). Moesin/CCS co-localization does not appear to be dependent on a direct moesin-clathrin interaction, because the consensus clathrin-binding domain, the LLpL(−) clathrin box motif (29), is absent in the primary structure of moesin, and the 4K/4N-moesin-GFP mutant that is unable to bind to PIP_2 does not co-distribute with CCSs. Therefore, the spatial localization of moesin within CCSs mainly depends on its N-terminal-PIP_2-binding domain that could interact with CCS-associated PIP_2.

Cells overexpressing the dominant-negative N-moesin-GFP molecule, unable to bind F-actin, presented abnormal clusters of CCSs as was similarly observed in moesin-silenced cells. In addition, the inert C-moesin-GFP molecule, which only binds to F-actin, does not co-localize with CCSs and does not affect their motility and cellular distribution. FL-moesin-GFP molecules distribute with preformed LCa-DsRed-labeled CCSs on plasma membrane, where the actin-linker moved out in the *z* axis direction associated with LCa-DsRed-labeled nascent CCVs. These data suggest that moesin regulates cellular dis-

tribution and lateral movement of a subpopulation of CCVs in an actin-dependent manner.

It has been suggested that actin plays either a structural role in clathrin-mediated endocytosis, controlling the localization of endocytic machinery on the plasma membrane, or the following mechanical roles: driving invagination, the separation of vesicles from the plasma membrane, and/or the translocation of nascent vesicles into the cytoplasm (57–59). For instance, the inhibition of actin dynamics blocks the internalization and lateral motility of a subpopulation of CCVs, which are differentially sensitive to actin disruption (60). Actin polymerization at endocytic sites is an early event that occurs during invagination of CCPs (21) and requires the cooperative contribution of several actin-associated proteins that allows the formation and endocytosis of nascent CCVs (reviewed in Refs. 21, 56–59, and 61–64). Hence, vesicle scission depends on the activity of the large GTPase dynamin that is recruited early on during CCP formation (21) and accumulates before vesicle pinching off (48, 65). A phenomenon that naturally follows vesicle scission is the recruitment of cortactin that binds to dynamin and F-actin (8, 66) and activates the Arp2/3 complex (8, 64), which is responsible for nucleation of actin polymerization (67). Therefore, it is thought that cortactin may link actin rearrangements with dynamin-mediated vesicle scission. A number of other endocytic proteins, including intersectin-1, huntingtin-interacting proteins, syndapin, the superfamily of Bin-Amphiphysin-Rvs proteins, which bind to dynamin, synaptojanin, or to the Arp2/3 activator neuronal Wiskott-Aldrich syndrome protein, and the Abi1 and neuronal Wiskott-Aldrich syndrome proteins have been shown to interact directly or indirectly with cortical actin to regulate CCV formation and related functions (5, 9, 68–77). Therefore, our data add complexity to this picture and provide evidence for the functional contribution of moesin, through binding to F-actin and CCS-associated PIP_2, in controlling lateral motility and cellular distribution of a subpopulation of moesin-associated CCVs.

It is conceivable that the hydrolisis of CCV-associated PIP_2, which could be performed by inositol-5-phosphatase synaptojanin (78–83), or its conversion to PIP_3 may represent a control mechanism for moesin-CCS association. This event may account for the partial moesin/CCS co-distribution observed in the present work. Thus, molecules that may directly or indirectly affect the ability of moesin to bind to actin or CCS-associated PIP_2 are potential candidates for the control of moesin-dependent trafficking of nascent endocytic CCVs.

Rab proteins, which constitute the largest family of monomeric small GTPases (84), have been identified as key regulators of intracellular transport at the endosome level (46, 85). We have observed that moesin knockdown provokes the accumulation of CCVs carrying the rab5 molecule, which represent nascent endocytic CCVs, and were not detected in plasma-membrane sheets.

Therefore, it appears that nascent rab5-CCVs require functional moesin to traffic correctly, after vesicle fission from plasma membrane. The functional perturbation of moesin may alter the trafficking of cargos associated with moesin-bearing CCVs as the constitutive associated TfR. TIRFM comparative studies, between intact cells and plasma-membrane sheets,

together with biochemical cell fractionation indicate that moesin silencing induces the accumulation of the TfR in endocytic rab5-CCVs. These data correlate with a reduced cell-surface expression of the TfR, determined by flow cytometry analysis and TIRFM-based studies, and the increase in the amount of the sequestered Tf ligand, which are indicative of a recycling defect of the TfR. Moreover, the presence of rab5-negative CCPs and deeply invaginated rab5/CCSs, equally detected in control and moesin-silenced plasma-membrane sheets, indicates that moesin does not affect either CCP formation or CCV invagination and fission from the plasma membrane. Hence, the Tf uptake is not affected during the first TfR internalization step in cells without moesin. Because TfR turnover is a constitutive process governed by the trafficking of endocytic CCVs (86), and considering that moesin knockdown does not appear to affect the frequency of TfR exocytosis to the plasma membrane, we propose that TfR recycling could be controlled in endocytic rab5-CCVs by signals affecting the functional status of moesin.

Interestingly, some members of the newly identified family of rab11 interacting proteins (rab11-FIP) possess an ERM domain in their C-terminal half of the molecule (87), which regulates FIP molecular self-interactions or interactions with rab11 GTPase during trafficking (88). Hence, it is possible that moesin may also regulate CCV trafficking by interacting with rab11-FIP members, thus perturbing FIP self-association or rab11-FIP/rab interactions.

In conclusion, we describe for the first time that moesin co-distributes with plasma membrane-derived CCSs, mostly in a PIP_2-dependent manner. The moesin protein controls lateral motility, cellular distribution, and trafficking of a subpopulation of nascent rab5-CCVs, probably promoting CCV recycling, through its ability to simultaneously bind to CCV-associated PIP_2 and F-actin.

These data represent an important mechanistic insight regarding the complex molecular machinery associated with CCSs, which drives clathrin-mediated endocytosis, and the functional involvement of moesin in the trafficking of CCVs. The study of cell signals or genetic mutations that regulate moesin activation might be important to understand the molecular basis of several pathological processes like cancer progression, congenital disorders of the central nervous system, and viral infection, all of which are reported to be associated with altered clathrin-mediated receptor internalization or recycling (89–92).

REFERENCES

1. Maldonado-Baez, L., and Wendland, B. (2006) *Trends Cell Biol.* **16,** 505–513
2. Ungewickell, E. J., and Hinrichsen, L. (2007) *Curr. Opin. Cell Biol.* **19,** 417–425

3. Le Borgne, R., Bardin, A., and Schweisguth, F. (2005) *Development* **132,** 1751–1762
4. Le Roy, C., and Wrana, J. L. (2005) *Nat. Rev. Mol. Cell. Biol.* **6,** 112–126
5. Benesch, S., Polo, S., Lai, F. P., Anderson, K. I., Stradal, T. E., Wehland, J., and Rottner, K. (2005) *J. Cell Sci.* **118,** 3103–3115
6. Scott, M. G., Benmerah, A., Muntaner, O., and Marullo, S. (2002) *J. Biol. Chem.* **277,** 3552–3559
7. Slepnev, V. I., and De Camilli, P. (2000) *Nat. Rev. Neurosci.* **1,** 161–172
8. Merrifield, C. J., Perrais, D., and Zenisek, D. (2005) *Cell* **121,** 593–606
9. Schafer, D. A. (2002) *Curr. Opin. Cell Biol.* **14,** 76–81
10. Laroche, G., Rochdi, M. D., Laporte, S. A., and Parent, J. L. (2005) *J. Biol. Chem.* **280,** 23215–23224
11. Hirasawa, A., Awaji, T., Sugawara, T., Tsujimoto, A., and Tsujimoto, G. (1998) *Br. J. Pharmacol.* **124,** 55–62
12. Lunn, J. A., Wong, H., Rozengurt, E., and Walsh, J. H. (2000) *Am. J. Physiol. Cell Physiol.* **279,** C2019–2027
13. Zaslaver, A., Feniger-Barish, R., and Ben-Baruch, A. (2001) *J. Immunol.* **166,** 1272–1284
14. Cao, H., Orth, J. D., Chen, J., Weller, S. G., Heuser, J. E., and McNiven, M. A. (2003) *Mol. Cell. Biol.* **23,** 2162–2170
15. Mangeat, P., Roy, C., and Martin, M. (1999) *Trends Cell Biol.* **9,** 187–192
16. Bretscher, A., Edwards, K., and Fehon, R. G. (2002) *Nat. Rev. Mol. Cell. Biol.* **3,** 586–599
17. Stanasila, L., Abuin, L., Diviani, D., and Cotecchia, S. (2006) *J. Biol. Chem.* **281,** 4354–4363
18. Cao, T. T., Deacon, H. W., Reczek, D., Bretscher, A., and von Zastrow, M. (1999) *Nature* **401,** 286–290
19. Li, J. G., Chen, C., and Liu-Chen, L. Y. (2002) *J. Biol. Chem.* **277,** 27545–27552
20. Harder, T., Kellner, R., Parton, R. G., and Gruenberg, J. (1997) *Mol. Biol. Cell* **8,** 533–545
21. Merrifield, C. J., Feldman, M. E., Wan, L., and Almers, W. (2002) *Nat. Cell Biol.* **4,** 691–698
22. Amieva, M. R., Litman, P., Huang, L., Ichimaru, E., and Furthmayr, H. (1999) *J. Cell Sci.* **112,** 111–125
23. Stauffer, T. P., Ahn, S., and Meyer, T. (1998) *Curr. Biol.* **8,** 343–346
24. Varnai, P., and Balla, T. (1998) *J. Cell Biol.* **143,** 501–510
25. Marin-Vicente, C., Gomez-Fernandez, J. C., and Corbalan-Garcia, S. (2005) *Mol. Biol. Cell* **16,** 2848–2861
26. Sever, S., Damke, H., and Schmid, S. L. (2000) *J. Cell Biol.* **150,** 1137–1148
27. Gaidarov, I., Santini, F., Warren, R. A., and Keen, J. H. (1999) *Nat. Cell Biol.* **1,** 1–7
28. Burns, A. R., Oliver, J. M., Pfeiffer, J. R., and Wilson, B. S. (2008) *Methods Mol. Biol.* **440,** 235–245
29. Kirchhausen, T. (2000) *Annu. Rev. Biochem.* **69,** 699–727
30. Musacchio, A., Smith, C. J., Roseman, A. M., Harrison, S. C., Kirchhausen, T., and Pearse, B. M. (1999) *Mol. Cell* **3,** 761–770
31. Ybe, J. A., Brodsky, F. M., Hofmann, K., Lin, K., Liu, S. H., Chen, L., Earnest, T. N., Fletterick, R. J., and Hwang, P. K. (1999) *Nature* **399,** 371–375
32. Brodsky, F. M., Chen, C. Y., Knuehl, C., Towler, M. C., and Wakeham, D. E. (2001) *Annu. Rev. Cell Dev. Biol.* **17,** 517–568
33. Conner, S. D., and Schmid, S. L. (2003) *Nature* **422,** 37–44
34. Schmid, S. L. (1997) *Annu. Rev. Biochem.* **66,** 511–548
35. Knuehl, C., Chen, C. Y., Manalo, V., Hwang, P. K., Ota, N., and Brodsky, F. M. (2006) *Traffic* **7,** 1688–1700
36. Robinson, M. S. (2004) *Trends Cell Biol.* **14,** 167–174
37. Kirchhausen, T. (2002) *Cell* **109,** 413–416
38. Boehm, M., and Bonifacino, J. S. (2001) *Mol. Biol. Cell* **12,** 2907–2920
39. Meyer, C., Zizioli, D., Lausmann, S., Eskelinen, E. L., Hamann, J., Saftig, P., von Figura, K., and Schu, P. (2000) *EMBO J.* **19,** 2193–2203
40. Engqvist-Goldstein, A. E., Warren, R. A., Kessels, M. M., Keen, J. H., Heuser, J., and Drubin, D. G. (2001) *J. Cell Biol.* **154,** 1209–1223
41. Franck, Z., Gary, R., and Bretscher, A. (1993) *J. Cell Sci.* **105,** 219–231
42. Ivetic, A., and Ridley, A. J. (2004) *Immunology* **112,** 165–176
43. Fievet, B. T., Gautreau, A., Roy, C., Del Maestro, L., Mangeat, P., Louvard, D., and Arpin, M. (2004) *J. Cell Biol.* **164,** 653–659
44. Nakamura, F., Huang, L., Pestonjamasp, K., Luna, E. J., and Furthmayr, H. (1999) *Mol. Biol. Cell* **10,** 2669–2685
45. Barret, C., Roy, C., Montcourrier, P., Mangeat, P., and Niggli, V. (2000) *J. Cell Biol.* **151,** 1067–1080
46. Zerial, M., and McBride, H. (2001) *Nat. Rev. Mol. Cell. Biol.* **2,** 107–117
47. Ullrich, O., Reinsch, S., Urbe, S., Zerial, M., and Parton, R. G. (1996) *J. Cell Biol.* **135,** 913–924
48. Ehrlich, M., Boll, W., Van Oijen, A., Hariharan, R., Chandran, K., Nibert, M. L., and Kirchhausen, T. (2004) *Cell* **118,** 591–605
49. Rappoport, J. Z., Simon, S. M., and Benmerah, A. (2004) *Traffic* **5,** 327–337
50. Keyel, P. A., Watkins, S. C., and Traub, L. M. (2004) *J. Biol. Chem.* **279,** 13190–13204
51. Rappoport, J. Z., Benmerah, A., and Simon, S. M. (2005) *Traffic* **6,** 539–547
52. McLauchlan, H., Newell, J., Morrice, N., Osborne, A., West, M., and Smythe, E. (1998) *Curr. Biol.* **8,** 34–45
53. Aisen, P. (2004) *Int. J. Biochem. Cell. Biol.* **36,** 2137–2143
54. Miesenbock, G., De Angelis, D. A., and Rothman, J. E. (1998) *Nature* **394,** 192–195
55. Sankaranarayanan, S., De Angelis, D., Rothman, J. E., and Ryan, T. A. (2000) *Biophys. J.* **79,** 2199–2208
56. Perrais, D., and Merrifield, C. J. (2005) *Dev. Cell* **9,** 581–592
57. Qualmann, B., Kessels, M. M., and Kelly, R. B. (2000) *J. Cell Biol.* **150,** F111–F116
58. Engqvist-Goldstein, A. E., and Drubin, D. G. (2003) *Annu. Rev. Cell Dev. Biol.* **19,** 287–332
59. Merrifield, C. J. (2004) *Trends Cell Biol.* **14,** 352–358
60. Yarar, D., Waterman-Storer, C. M., and Schmid, S. L. (2005) *Mol. Biol. Cell* **16,** 964–975
61. Girao, H., Geli, M. I., and Idrissi, F. Z. (2008) *FEBS Lett.* **582,** 2112–2119
62. Lanzetti, L. (2007) *Curr. Opin. Cell Biol.* **19,** 453–458
63. Kaksonen, M., Toret, C. P., and Drubin, D. G. (2006) *Nat. Rev. Mol. Cell. Biol.* **7,** 404–414
64. Merrifield, C. J., Qualmann, B., Kessels, M. M., and Almers, W. (2004) *Eur. J. Cell Biol.* **83,** 13–18
65. Zoncu, R., Perera, R. M., Sebastian, R., Nakatsu, F., Chen, H., Balla, T., Ayala, G., Toomre, D., and De Camilli, P. V. (2007) *Proc. Natl. Acad. Sci. U. S. A.* **104,** 3793–3798
66. Daly, R. J. (2004) *Biochem. J.* **382,** 13–25
67. Takenawa, T., and Miki, H. (2001) *J. Cell Sci.* **114,** 1801–1809
68. McPherson, P. S. (2002) *Trends Cell Biol.* **12,** 312–315
69. Itoh, T., Erdmann, K. S., Roux, A., Habermann, B., Werner, H., and De Camilli, P. (2005) *Dev. Cell* **9,** 791–804
70. Tsujita, K., Suetsugu, S., Sasaki, N., Furutani, M., Oikawa, T., and Takenawa, T. (2006) *J. Cell Biol.* **172,** 269–279
71. Dawson, J. C., Legg, J. A., and Machesky, L. M. (2006) *Trends Cell Biol.* **16,** 493–498
72. Takenawa, T., and Suetsugu, S. (2007) *Nat. Rev. Mol. Cell. Biol.* **8,** 37–48
73. Innocenti, M., Gerboth, S., Rottner, K., Lai, F. P., Hertzog, M., Stradal, T. E., Frittoli, E., Didry, D., Polo, S., Disanza, A., Benesch, S., Di Fiore, P. P., Carlier, M. F., and Scita, G. (2005) *Nat. Cell Biol.* **7,** 969–976
74. Chen, C. Y., and Brodsky, F. M. (2005) *J. Biol. Chem.* **280,** 6109–6117
75. Le Clainche, C., Pauly, B. S., Zhang, C. X., Engqvist-Goldstein, A. E., Cunningham, K., and Drubin, D. G. (2007) *EMBO J.* **26,** 1199–1210
76. Wilbur, J. D., Chen, C. Y., Manalo, V., Hwang, P. K., Fletterick, R. J., and Brodsky, F. M. (2008) *J. Biol. Chem.* **283,** 32870–32879
77. Qualmann, B., and Kelly, R. B. (2000) *J. Cell Biol.* **148,** 1047–1062
78. McPherson, P. S., Garcia, E. P., Slepnev, V. I., David, C., Zhang, X., Grabs, D., Sossin, W. S., Bauerfeind, R., Nemoto, Y., and De Camilli, P. (1996) *Nature* **379,** 353–357
79. Cremona, O., Di Paolo, G., Wenk, M. R., Luthi, A., Kim, W. T., Takei, K., Daniell, L., Nemoto, Y., Shears, S. B., Flavell, R. A., McCormick, D. A., and De Camilli, P. (1999) *Cell* **99,** 179–188
80. Haffner, C., Takei, K., Chen, H., Ringstad, N., Hudson, A., Butler, M. H., Salcini, A. E., Di Fiore, P. P., and De Camilli, P. (1997) *FEBS Lett.* **419,** 175–180
81. Harris, T. W., Hartwieg, E., Horvitz, H. R., and Jorgensen, E. M. (2000) *J. Cell Biol.* **150,** 589–600
82. Verstreken, P., Koh, T. W., Schulze, K. L., Zhai, R. G., Hiesinger, P. R., Zhou, Y., Mehta, S. Q., Cao, Y., Roos, J., and Bellen, H. J. (2003) *Neuron* **40,**

733–748

83. Gad, H., Ringstad, N., Low, P., Kjaerulff, O., Gustafsson, J., Wenk, M., Di Paolo, G., Nemoto, Y., Crun, J., Ellisman, M. H., De Camilli, P., Shupliakov, O., and Brodin, L. (2000) *Neuron* **27,** 301–312

84. Bock, J. B., Matern, H. T., Peden, A. A., and Scheller, R. H. (2001) *Nature* **409,** 839–841

85. Rink, J., Ghigo, E., Kalaidzidis, Y., and Zerial, M. (2005) *Cell* **122,** 735–749

86. Daniels, T. R., Delgado, T., Rodriguez, J. A., Helguera, G., and Penichet, M. L. (2006) *Clin. Immunol.* **121,** 144–158

87. Lindsay, A. J., and McCaffrey, M. W. (2004) *J. Cell Sci.* **117,** 4365–4375

88. Wallace, D. M., Lindsay, A. J., Hendrick, A. G., and McCaffrey, M. W. (2002) *Biochem. Biophys. Res. Commun.* **299,** 770–779

89. Polo, S., Pece, S., and Di Fiore, P. P. (2004) *Curr. Opin. Cell Biol.* **16,** 156–161

90. Cataldo, A. M., Peterhoff, C. M., Troncoso, J. C., Gomez-Isla, T., Hyman, B. T., and Nixon, R. A. (2000) *Am. J. Pathol.* **157,** 277–286

91. Venkatesan, S., Rose, J. J., Lodge, R., Murphy, P. M., and Foley, J. F. (2003) *Mol. Biol. Cell* **14,** 3305–3324

92. Connor, J. R., Wang, X. S., Patton, S. M., Menzies, S. L., Troncoso, J. C., Earley, C. J., and Allen, R. P. (2004) *Neurology* **62,** 1563–1567